iScience

CellPress

Article

# RARβ Agonist Drug (C286) Demonstrates Efficacy in a Pre-clinical Neuropathic Pain Model Restoring Multiple Pathways via DNA Repair Mechanisms

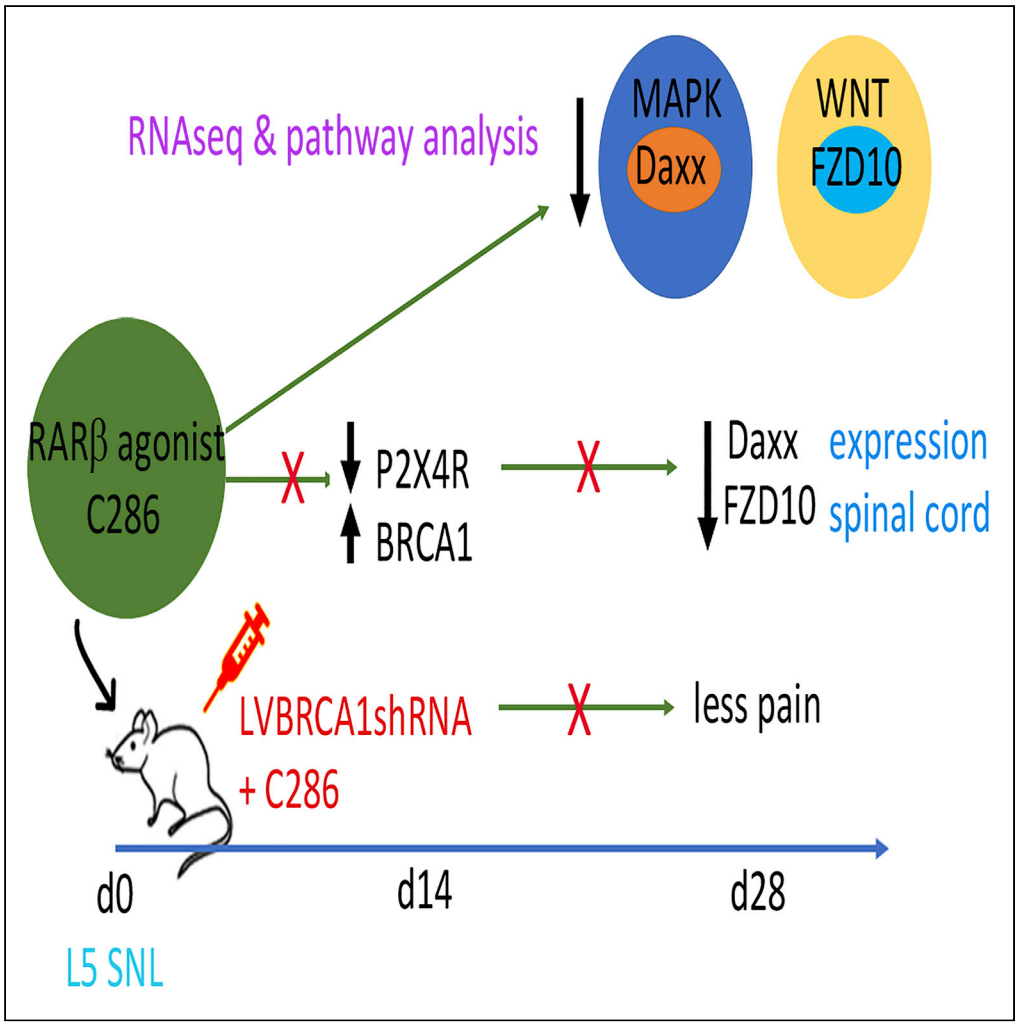


Maria B. Goncalves, Julien Moehlin, Earl Clarke, ..., Julian Jack, Marco Antonio Mendoza-Parra, Jonathan P.T. Corcoran

bia.goncalves@kcl.ac.uk (M.B.G.)
mmendoza@genoscope.cns.fr (M.A.M.-P.)
jonathan.corcoran@kcl.ac.uk (J.P.T.C.)

## HIGHLIGHTS

RARβ drug (C286) prevents neuropathic pain after nerve injury

C286 restores multiple pain pathways to preinjury levels, including MAPK and WNT

C286 modulates the DNA repair mechanisms BRCA1 and ATM

BRCA1 is required for C286's effects in neuropathic pain

Goncalves et al., iScience *20*, 554–566
October 25, 2019 
https://doi.org/10.1016/j.isci.2019.09.020

iScience

CellPress

Article

# RARβ Agonist Drug (C286) Demonstrates Efficacy in a Pre-clinical Neuropathic Pain Model Restoring Multiple Pathways via DNA Repair Mechanisms

Maria B. Goncalves,[1,4,*] Julien Moehlin,[2] Earl Clarke,[1] John Grist,[1] Carl Hobbs,[1] Antony M. Carr,[3] Julian Jack,[1] Marco Antonio Mendoza-Parra,[2,*] and Jonathan P.T. Corcoran[1,*]

## SUMMARY

**Neuropathic pain (NP) is associated with profound gene expression alterations within the nociceptive system. DNA mechanisms, such as epigenetic remodeling and repair pathways have been implicated in NP. Here we have used a rat model of peripheral nerve injury to study the effect of a recently developed RARβ agonist, C286, currently under clinical research, in NP. A 4-week treatment initiated 2 days after the injury normalized pain sensation. Genome-wide and pathway enrichment analysis showed that multiple mechanisms persistently altered in the spinal cord were restored to preinjury levels by the agonist. Concomitant upregulation of DNA repair proteins, ATM and BRCA1, the latter being required for C286-mediated pain modulation, suggests that early DNA repair may be important to prevent phenotypic epigenetic imprints in NP. Thus, C286 is a promising drug candidate for neuropathic pain and DNA repair mechanisms may be useful therapeutic targets to explore.**

## INTRODUCTION

The identification of an effective therapy for neuropathic pain (NP) has been challenging owing to three main factors: first, multiple mechanisms are involved for which no single multifactorial drug has been developed; second, differences in cellular and molecular mechanisms between animals and humans have hampered progress; and third, no single "switch" has been identified that could curtail the pathological cascade and provide a therapeutic target (Borsook et al., 2014; Gereau et al., 2014).

There are two primary features of NP: (1) hyperalgesia, increased pain from a stimulus that usually evokes pain; and (2) allodynia, pain due to a stimulus that usually does not provoke pain (Jensen and Finnerup, 2014). It appears that there are at least two distinct aspects to the development of these features: peripheral sensitization, involving changes in the threshold of peripheral nociceptors including possible spontaneous firing, and central sensitization, in which there are changes in the responsiveness at the central synapses relaying nociception, especially in the dorsal horn of the spinal cord. There is still debate about the importance of central sensitization and whether it relies, for its maintenance, on the peripherally sensitized input (Meacham et al., 2017).

Although it is generally agreed that there are a profusion of gene expression changes in NP (Descalzi et al., 2015), the underlying general mechanism by which they are induced is still uncertain. One suggestion is that the underlying cause is an inflammatory reaction to injury (Ellis and Bennett, 2013), which in turn causes DNA damage (Kelley and Fehrenbacher, 2017). Madabhushi and colleagues (Madabhushi et al., 2015) have shown that even neuronal activity can be sufficient to induce DNA damage (double-strand breaks, DSBs), particularly in the promoter region of early response genes, causing their upregulation, and this, in turn, can alter the expression of late response genes, such as brain-derived neurotrophic factor (*bdnf*). Their experiments supported the conclusion that DNA DSB formation was necessary and sufficient to induce early response gene expression and that DNA repair could reverse the gene expression. Similarly, Fehrenbacher and her colleagues showed that enhanced DNA repair could reverse the changes in neuronal sensitivity that they observed (Kelley and Fehrenbacher, 2017).

In terms of cellular responses, converging lines of evidence support that a specific microglia inflammatory phenotype characterized by the *de novo* expression of the purinergic receptor P2X4 is critical to the

[1]The Wolfson Centre for Age-Related Diseases, King's College London, Guy's Campus, London SE1 1UL, UK

[2]Génomique Métabolique, Genoscope, Institut François Jacob, CEA, CNRS, Univ Evry, Université Paris-Saclay, 91057 Evry, France

[3]Genome Damage and Stability Centre, School of Life Sciences, University of Sussex, Brighton BN1 9RQ, UK

[4]Lead Contact

*Correspondence: bia.goncalves@kcl.ac.uk (M.B.G.), mmendoza@genoscope.cns.fr (M.A.M.-P.), jonathan.corcoran@kcl.ac.uk (J.P.T.C.)

https://doi.org/10.1016/j.isci.2019.09.020

induction of core pain signaling, mediated by the release of BDNF, which produces hypersensitivity in nociceptive neuron in the spinal dorsal horn.

It is not understood how this specific spinal microglia phenotype ($P2X4R^+$) that arises during the acute stage following peripheral nerve injury (PNI) results in imprinting of the chronic and persistent changes in the spinal nociceptive networks after the acute inflammatory response has subsided (Beggs et al., 2012; Ulmann et al., 2013). Epigenetic alterations in spinal microglia during the acute inflammatory response presents a favorable paradigm for the imprinting mechanism driving chronicity of the pain state (Denk et al., 2016) because of the high transcriptional activity induced by the inflammatory response and the associated increase in DNA DSB (Marnef et al., 2017). Indeed, a wealth of data suggests that the fragility of actively transcribing loci is intertwined with genomic changes that are linked to altered cellular function and disease (Alt and Schwer, 2018; Fong et al., 2013; Puc et al., 2017; Sharma et al., 2015; Su et al., 2015). This raises the question: could this represent a biological switch and thus a therapeutic target, whereby inducing an increase in DNA repair following PNI would preserve the genomic landscape of the spinal microglia during acute activation, when high transcriptional activity is expected, and thus provide an effective way to target NP?

Here we show that a novel drug, Retinoic Acid Receptor (RAR)β agonist, C286 (Goncalves et al., 2019a), prevents NP by restoring pathways that are chronically altered in the spinal cord (SC) after PNI and that this is associated with a switch in the spinal microglia P2X4R phenotype via a mechanism dependent on the breast cancer susceptibility gene 1 (BRCA1). Since the retinoic acid (RA) pathway is highly conserved between species (Rhinn and Dolle, 2012), our findings support C286 as a plausible impending therapy for NP and provide evidence that DNA repair mechanisms are disease-modifying therapeutic targets.

## RESULTS

### C286 Modulates Multiple Pathways Chronically Altered after Spinal Nerve Ligation

RA has been shown to inhibit TNFα and iNOS in reactive microglia (Dheen et al., 2005), and our previous work shows that stimulation of RARβ hampers astrogliosis after spinal cord injury (Goncalves et al., 2015). We therefore hypothesized that a novel drug RARβ agonist, C286, may modulate the inflammatory response of activated microglia to prevent the onset of the microglia-neuron alterations that underly NP. Because we specifically wanted to investigate the effect of the drug in $P2X4R^+$ microglia and this phenotype has been shown to evoke spinal mechanisms of nerve injury-induced hypersensitivity predominantly in males but not in female rats (Mapplebeck et al., 2018), we chose male rats only for this study.

Using an established rat model of NP, L5 spinal nerve ligation (SNL) (Kim and Chung, 1992), we assessed the effect of C286 given orally for 4 weeks on mechanical and thermal pain thresholds over the treatment period. C286 treatment reversed the hypersensitivity caused by SNL to levels comparable with the preinjury state (Figures 1A–1E). We next used co-expression analysis of genome-wide RNA sequencing of dorsal horns isolated from non-injured and L5-SNL rats that had been treated with vehicle or C286 to delineate pathways that may have a role in the formation of the long-term hyperalgesia-related imprint in the SC (Figures 1F and 1G). The non-injured tissue was used to establish the normal gene expression with and without C286, whereas the L5-SNL vehicle-treated tissue served as a platform to identify gene expression patterns that were induced by the surgery and peripheral lesion and was used as a control to directly compare gene expression changes that were altered solely owing to the drug treatment. Through analysis of co-expression paths we identified a variety of genes involved in a broad range of cellular functions, including neural transmission, cell adhesion, growth cone and synapse formation, and mitochondrial function (Figure 1H). Among differentially expressed transcripts we identified genes associated with pain-related pathways, altered in different models of pain, or encoding products interacting with proteins involved in pain-related pathways (Figures S1 and S2 and Table S1 [related to Figures 1 and 2]. Figure S2 and Table S1 are available on the Mendeley repository https://doi.org/10.17632/kjvs5vgkbf.1DOI). We observed that C286 upregulates pathways that are compromised in NP: cell adhesion (Patil et al., 2011), growth cone (Hur et al., 2012), and gap junction (Wu et al., 2012) (Figure S2, https://doi.org/10.17632/kjvs5vgkbf.1DOI) and downregulates pathways back to non-injured baseline that are upregulated in NP: long-term potentiation (Ruscheweyh et al., 2011), WNT (Zhang et al., 2013), MAPK (Ji et al., 1999; Jiang et al., 2008; Jin et al., 2003; Kawasaki et al., 2004; Obata and Noguchi, 2004; Song et al., 2005; Zhang and Yang, 2017), erbB (Calvo et al., 2011), TRP channels (Moran and Szallasi, 2018), and cAMP (Edelmayer et al., 2014) (Figures 2A, 2B, and S2 and Table S1, available on the Mendeley repository https://doi.org/10.17632/kjvs5vgkbf.1DOI).

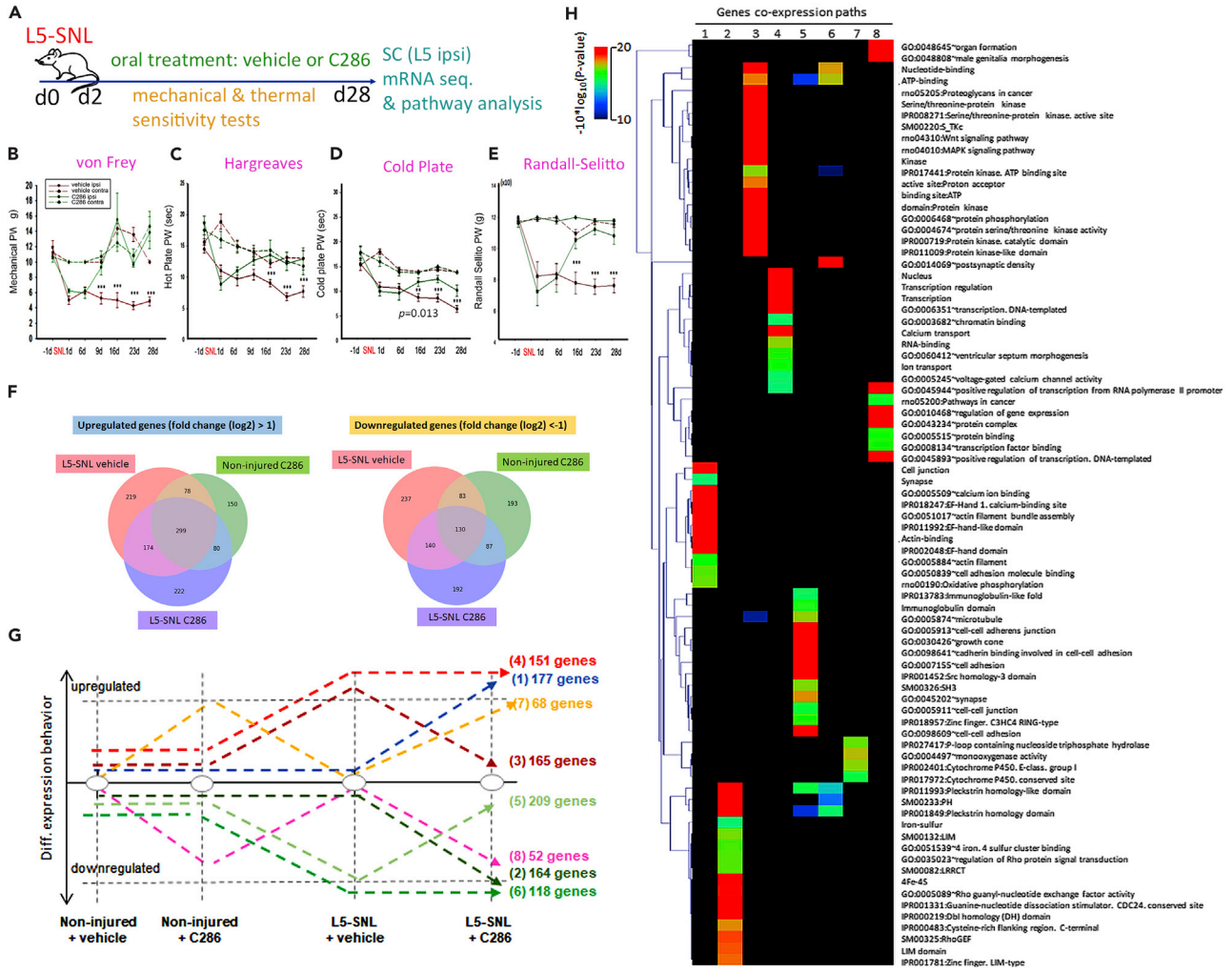


**Figure 1. C286 Modulates Multiple Pathways Chronically Altered after SNL**

(A–E) (A) Schematic of experimental paradigm. L5-SNL, spinal nerve ligation; SC L5 ipsi (spinal cord, L5 level ipsilateral to injury) indicates the area where tissue analysis was carried out and is delineated as a red square in subsequent figures. Measurement of mechanical and thermal sensitivities shown as paw withdrawal (PW) in grams (g) or seconds (sec), by (B) von Frey filaments, (C) hot plate, (D) cold plate, (E) and Randall Selitto test in vehicle ($n = 8$) or C286 ($n = 8$). Data shown as Mean ± SEM. Two-way ANOVA with Pairwise Multiple Comparison Procedures (Holm-Sidak method). $^{**}p \leq 0.01$, $^{***}p \leq 0.001$.
(F–H) Gene co-expression analysis assessed in the SC from L5-SNL rats and non-injured rats, treated with vehicle or C286. (F) Differential gene expression analysis relative to the sample non-injured + vehicle. (G) Differentially expressed genes are classified by their co-expression paths assessed after injury and injury + vehicle or C286 treatment. (H) Gene ontology analysis performed per co-expression path. The heatmap illustrates the GO enrichment confidence.

Because of their prominent role in the regulation of nociceptive signal perception we focused on the MAPK and WNT pathways for further analysis.

WNT signaling in the SC stimulates the production of proinflammatory cytokines through the activation of WNT/FZ/β-catenin pathway in nociceptive neurons (Tang, 2014; Zhang et al., 2013). MAPK is activated in spinal microglia after PNI and, upon nuclear translocation, activates transcription factors that promote dynamic nuclear remodeling. This results in the transcription and translation of proteins that prolong potentiation and decrease the threshold for receptor activation, the molecular underpinnings of clinical allodynia (Wahezi et al., 2015).

The WNT receptor Frizzled 10 (FZD10) and the death domain-associated protein, Daxx, components of the WNT and MAPK pathways, respectively, were highlighted by our co-expression analysis owing to the magnitude of their expression changes between vehicle and C286-treated L5-SNL rats. FZD10 has been

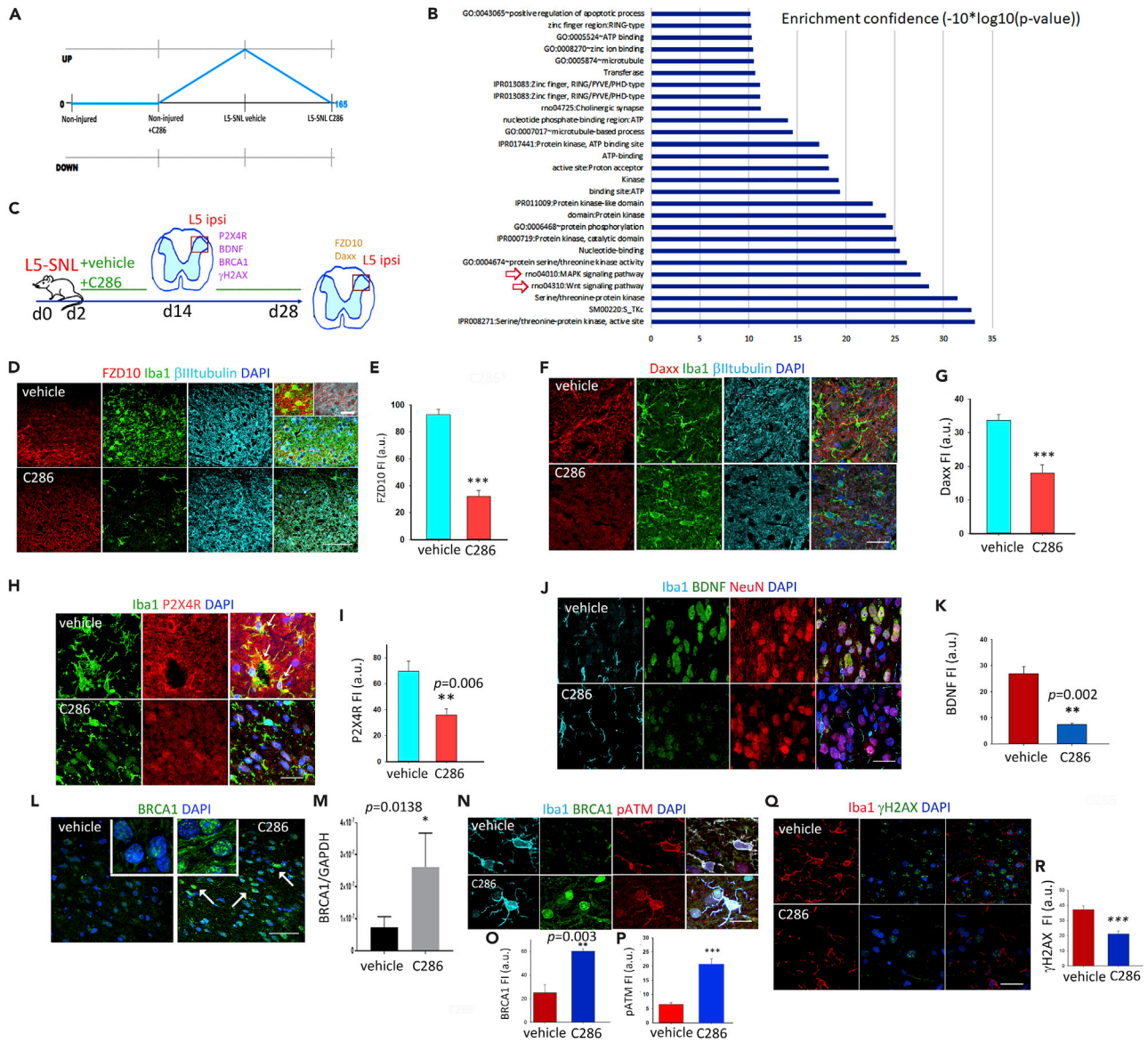


**Figure 2. C286 Regulates Inflammatory and DNA Repair Pathways**

(A) Genes were classified on the basis of their co-expression behavior over the various conditions. C286 downregulated 165 genes that had been upregulated by the injury.

(B) GO terms associated to the co-expressed genes are displayed on the basis of their confidence (−10*log10[p value]), red arrows highlight the MAPK and WNT pathways.

(C) Diagram of experimental design.

(D–G) (D and E) Representative images and quantification of FZD10 (scale bar, 100 μm and 20 μm for higher-magnification insets) and (F and G) of Daxx expression in microglia (Iba1) and neurons (βIII tubulin) in the SC at the end of the treatment period (scale bar, 50 μm). Two weeks after injury, a sub-set of vehicle- and C286-treated rats was used for immunohistological analysis ($n$ = 3 per treatment group) and for RT-qPCR ($n$ = 3 per treatment group).

(H–K) (H and I) Levels of P2X4R$^+$ microglia (highlighted by arrows in the merged upper panel, scale bar, 30 μm) and (J and K) BDNF (in neurons and microglia) in the SC (scale bar, 30 μm).

(L and M) (L) Images showing BRCA1 expression in the same area (insets show higher magnification of BRCA1 in nuclei, scale bar, 100 μm) and (M) quantification by RT-qPCR.

(N–P) Expression and quantification of BRCA1 and pATM in spinal microglia (scale bar, 20 μm).

(Q and R) Expression and quantification of γH2AX (scale bar, 100 μm).

In E, G, I, K, O, P, and R, data are shown as Mean ± SEM of fluorescence intensity (FI) in arbitrary units (a.u.). Student's t test, **p ≤ 0.01, ***p ≤ 0.001, $n$ = 4 (E and G) or $n$ = 3 (I, K, M, P, and R) per group, five sections per animal).

shown to be expressed in pain pathways, including dorsal horn neurons (Hu et al., 2009), and Daxx (which is ubiquitously expressed) has a well-established role in apoptosis but can also participate in numerous additional cellular functions as a mediator of protein interactions (Lindsay et al., 2008), as a potent suppressor of transcription (Takahashi et al., 2004), and as a modulator of cargo-loaded vesicles transport, an important emerging factor in neuron-glia cross-talk during NP (McDonald et al., 2014; Shiue et al., 2019). Immunohistochemistry confirmed downregulation of FZD10 and Daxx protein levels by C286 (see Figures 2C–2G).

### C286 Regulates Inflammatory and DNA Repair Pathways

Inflammation can be a common trigger of MAPK and WNT pathways (Roubert et al., 2017), and hence their downregulation by the agonist at 28 days post injury could indicate an earlier resolution of the inflammatory state. A subtype of purinergic receptor, P2X4R, regulates microglial activation (Ulmann et al., 2013), and its upregulation in spinal microglia has been proposed as an important inflammatory switch that is necessary and sufficient for subsequent pain hypersensitivity, acting via BDNF release and subsequent uptake by the nociceptive neurons in the dorsal horn (Beggs et al., 2012). We therefore assessed the effect of C286 on the expression of P2X4R in spinal microglia and BDNF in microglia and neurons in the dorsal horn at 14 days post PNI, a time point that reflects the interphase between the beneficial acute microglia response and the switch to the perpetuated reactive state that could trigger the chronic pain. We found both to be significantly lower compared with vehicle-treated rats (Figures 2H–2K). Similarly, other inflammatory mediators and growth factors associated with NP, such as NGF, TNF$\alpha$, and TNFR1 (Amaya et al., 2013), were also downregulated in the agonist-treated SCs (Figures S3A–S3H, related to Figure 2). We did not find their mRNAs upregulated at 4 weeks in the vehicle-treated L5-SNL rats, in agreement with other studies in the same injury model that report only a temporary post-lesion increase in these proteins (de Jager et al., 2011).

Next, we wanted to ascertain if the switch in the microglia phenotype from predominantly P2X4R$^{+}$ to P2X4R$^{-}$ correlated with higher DNA repair efficiency. We reasoned that an increase in DNA repair during the acute phase of microglia activation (Ellis and Bennett, 2013), when transcriptional changes are occurring during adaptation to the injury, could prevent the occurrence of transcriptional imprints that contribute to chronic pain. This would favor regaining the non-activated genomic state. The involvement of the DNA repair protein BRCA1 in spinal microglia after injury has been recently described where an initial physiological attempt to repair is seen by an increase in BRCA1 expression, but that is not sustained beyond 72 h post injury (Noristani et al., 2017). A link between BRCA1 and RA signaling has been highlighted by previous studies; genome-wide analysis suggests a role for BRCA1 in transcriptional co-activation to RA (Gardini et al., 2014) and RAR/RXR-mediated transcription requires recruitment of the BRCA1 co-repressor C-terminal-binding protein 2 (CtBP2) (Bajpe et al., 2013), which could result in the elevation of BRCA1 transcription, a mechanism already described for estrogen (Di et al., 2010).

To assess if C286 could be prolonging BRCA1 expression, we measured BRCA1 levels in the dorsal horn by western blotting (Figures 2L and 2M) and by immunochemistry in spinal microglia and found that C286 significantly increased BRCA1 levels, predominantly in the nucleus (Figures 2L, 2N, and 2O).

### C286 Regulates DNA Damage in Microglia via BRCA1 and ATM Pathways

Cellular responses to DNA damage are mediated by an extensive network of signaling pathways. The ataxia telangiectasia mutated (ATM) kinase responds specifically to DNA DSBs, which are associated with signal-induced transcriptional changes. ATM can be activated by RA (Fernandes et al., 2007) and suppresses MAPK pathways via a DSB-induced response whereby MKP-5 is upregulated and dephosphorylates and inactivates the stress-activated MAP kinases JNK and p38 (Bar-Shira et al., 2002). We therefore assessed ATM phosphorylation levels in the SCs and found that C286 significantly increased pATM in spinal microglia (Figures 2N and 2P). Concomitantly, we observed a significant decrease in the ATM target and DNA damage marker $\gamma$H2AX (Sharma et al., 2012) (Figures 2Q and 2R). To confirm if the modulation of these two DNA repair mechanisms was a direct effect of the agonist in microglia, we treated lipopolysaccharide-activated microglia cultures with vehicle, C286, an ATM inhibitor (KU55933) alone, or with C286 and found that C286 significantly increased BRCA1 and pATM and significantly decreased $\gamma$H2AX compared with vehicle. Importantly, the effect on pATM was completely abrogated in the presence of KU55933, suggesting a direct effect on ATM auto-phosphorylation (Figures 3A–3H).

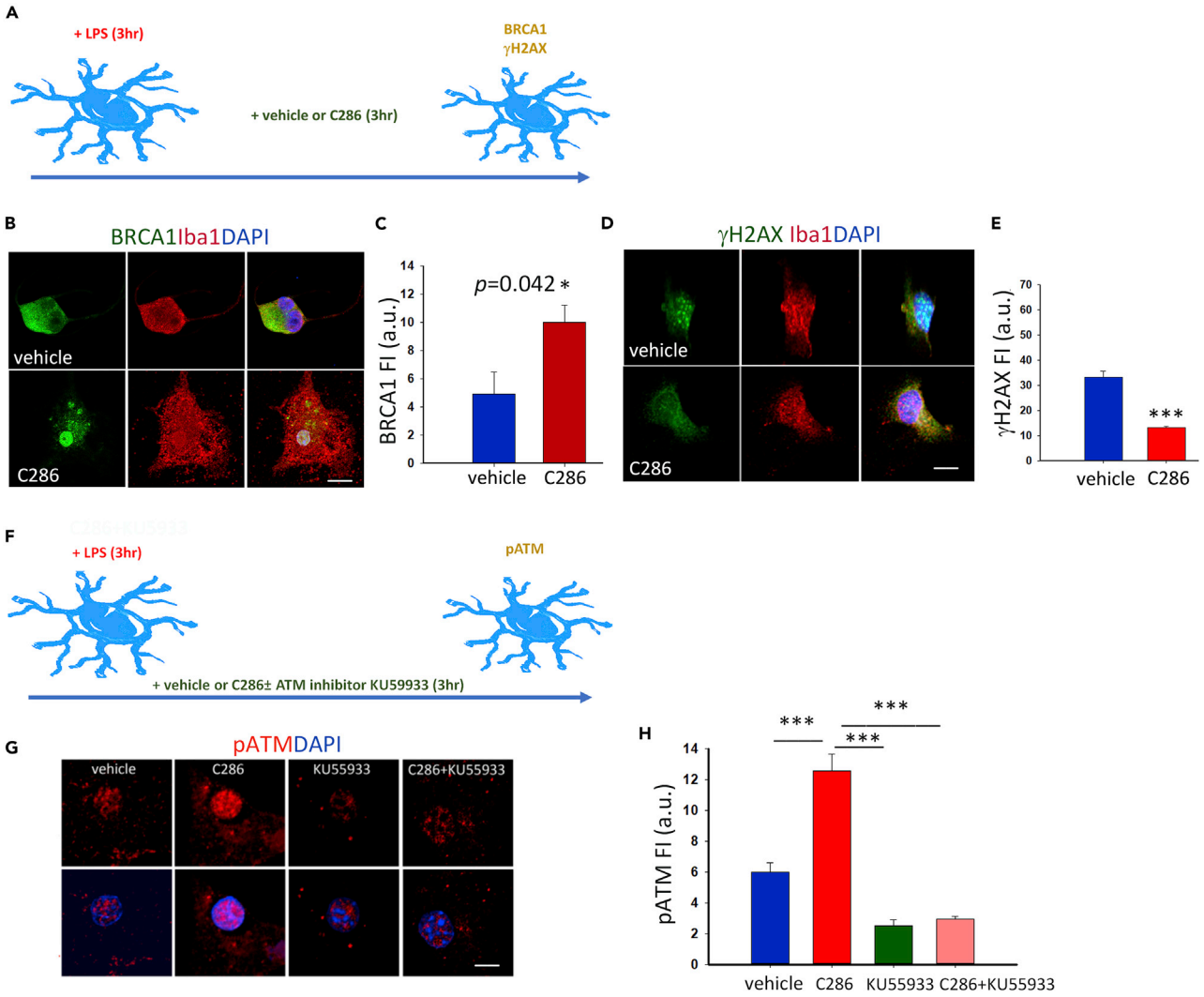


**Figure 3. C286 Regulates DNA Damage in Microglia via BRCA1 and ATM Pathways**

(A) Diagram showing microglia culture conditions and markers assessed.

(B–E) (B and C) BRCA1 and (D and E) γH2AX expression and quantification in microglia cultures.

(F) Diagram showing the experimental design.

(G and H) Expression and quantification of pATM in nuclei in the different culture conditions. Scale bars, 15 μm. Data show Mean FI ± SEM from three independent experiments (C and E), Student's t test, *$p \leq 0.05$ and (H) one-way ANOVA with Pairwise Multiple Comparison Procedures (Tukey Test), ***$p \leq 0.001$.

## BRCA1 Is a Downstream Target of C286 in NP Modulation

To functionally validate the RARβ-BRCA1 pathway in pain we used lentiviral transduction of shRNA BRCA1 in our rat model of NP. Treatment with C286 yielded no significant improvement in the pain thresholds when BRCA1 was ablated (Figures 4A–4C). Confirmation of effective lentiviral transduction was obtained by immunochemistry (Figures 4D–4F). Further analysis of BRCA1 expression in spinal microglia showed that this was significantly decreased in LV/BRCA1shRNA + C286-treated rats compared with LV/sc + C286 (Figures 4G–4I), and the inverse was seen with γH2AX (Figures 4J–4L). In agreement with the pain behavioral tests, we found that the calcitonin gene-related peptide (CGRP), which contributes to the hyper-sensitization (Iyengar et al., 2017), was significantly upregulated in the dorsal horn (predominantly laminae I-III) of LV/BRCA1shRNA + C286-treated rats (Figures 4M and 4N).

To establish if there was a direct link between BRCA1 and the microglia activation, we assessed the levels of P2X4R in spinal microglia and found a significant increase in the LV/BRCA1shRNA + C286-transduced rats

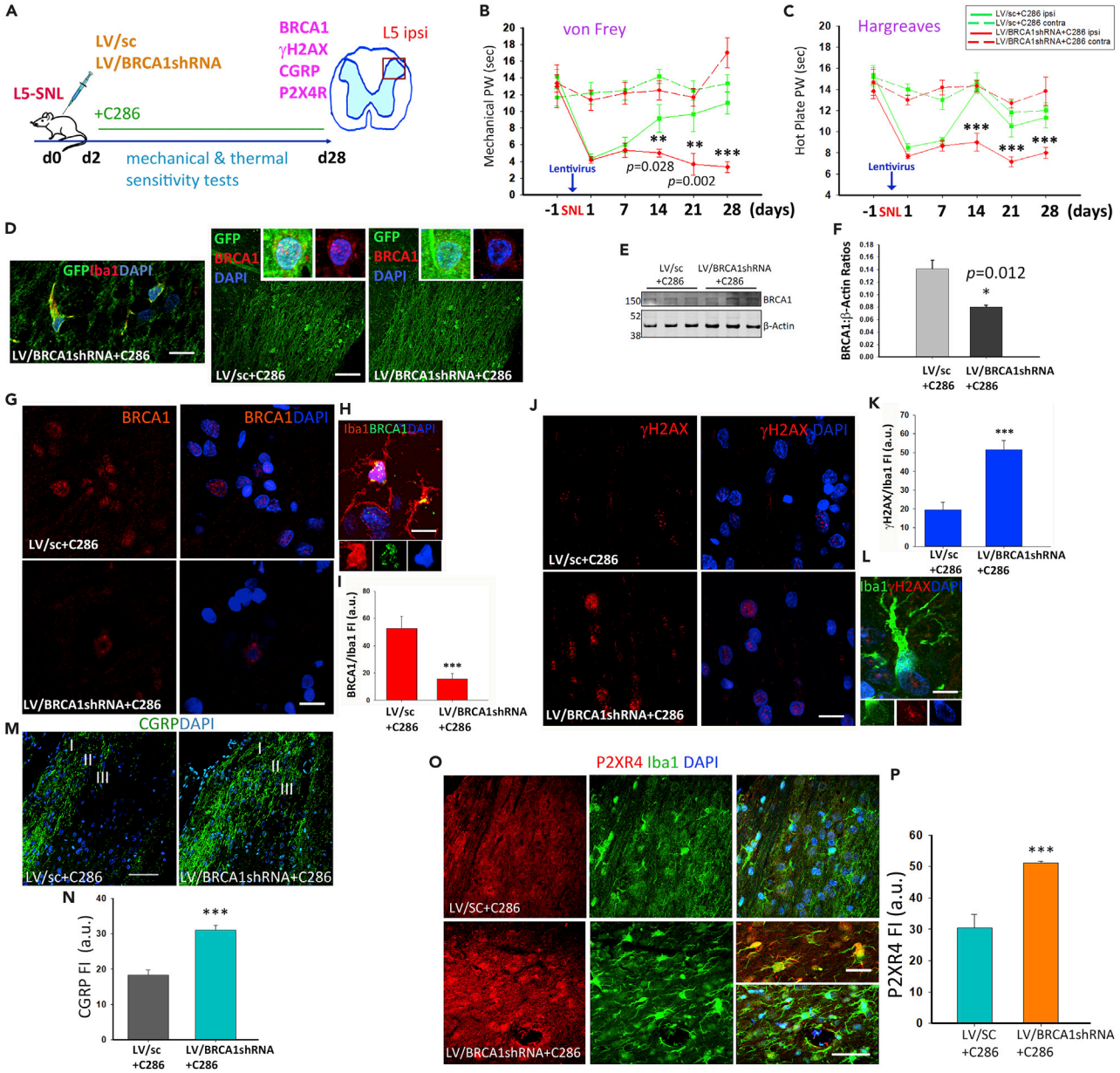


**Figure 4. BRCA1 Is a Downstream Target of C286 in NP Modulation**

(A) Schematic of experimental paradigm.

(B and C) (B) Measurement of thermal and mechanical sensitivities by von Frey filaments (C) and hot plate in vehicle ($n$ = 6) or C286 ($n$ = 6). Data shown as Mean ± SEM. Two-way ANOVA with Pairwise Multiple Comparison Procedures (Holm-Sidak method). ***p ≤ 0.001.

(D) Co-labelling of GFP and Iba1 (scale bar, 20 μm), and GFP and BRCA1 in LVsc + C286- and LVBRCA1shRNA + C286-treated rats (scale bar, 100 μm).

(E–H) (E and F) Western blots and quantification of BRCA1 in L5-SNL rats transduced with LV/SC + C286 ($n$ = 3) or LV/BRCA1shRNA + C286 ($n$ = 3). Student's t test. *p ≤ 0.05 (G) Immunohistological confirmation of LV transduction (scale bar, 20 μm), (H) higher-magnification inset shows BRCA1 in microglia in an LV/Sc + C286-treated rat (scale bar, 10 μm).

(I) Quantification of BRCA1 in microglia.

(J and K) Expression and quantification of γH2AX (scale bar, 20 μm), (L) higher-magnification inset shows γH2AX in microglia in an LV/BRCA1shRNA + C286-treated rat (scale bar, 10 μm).

(M and N) Expression and quantification of CGRP in laminae I–III of the dorsal horn (scale bar, 100 μm).

(O and P) Expression and quantification of P2X4R (scale bar, 100 μm). Inset shows higher-magnification image (scale bar, 20 μm) Data are shown as Mean +SEM of FI. Student's t test, **p ≤ 0.01, ***p ≤ 0.001 ($n$ = 3 per group, 5 sections per animal).

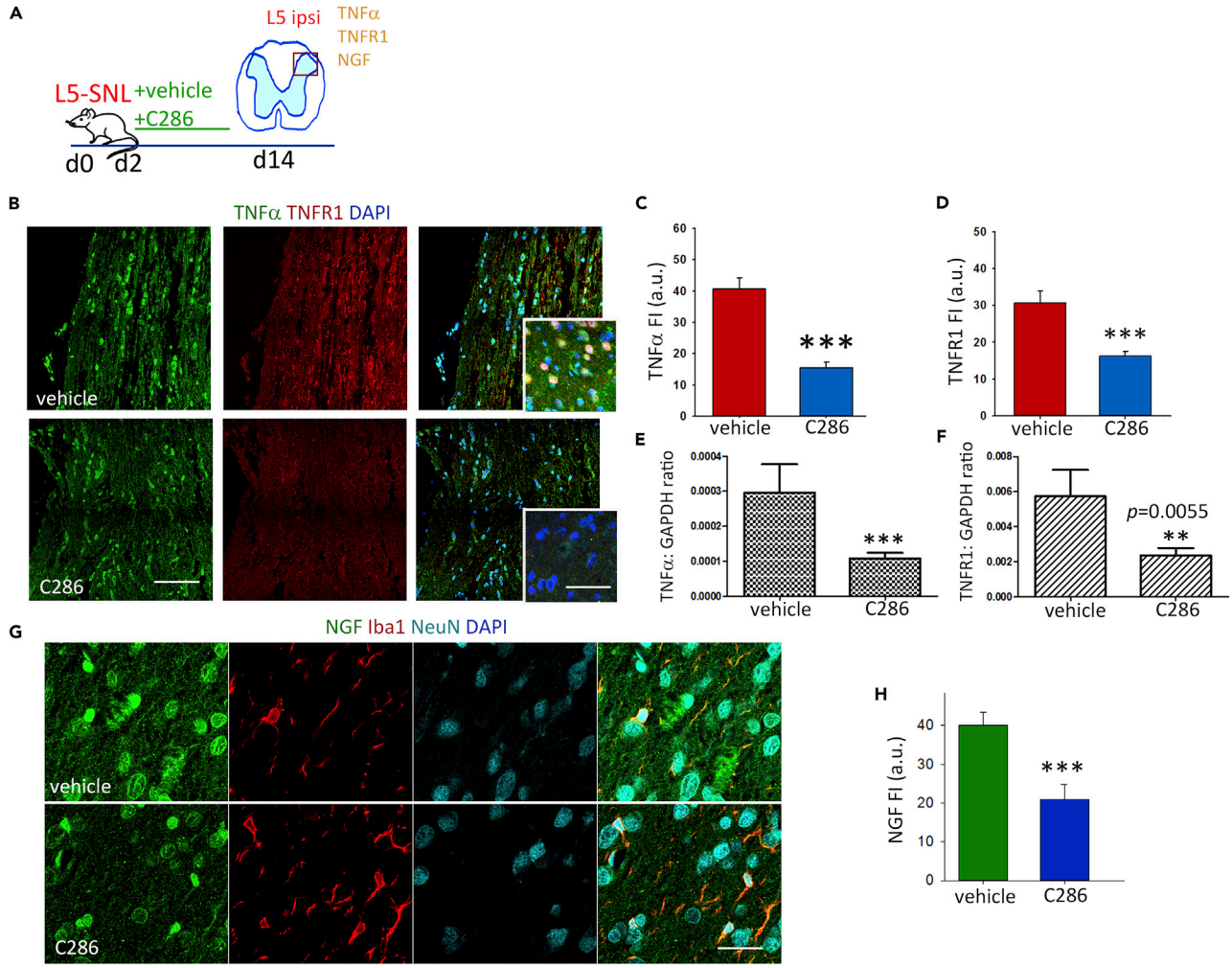


**Figure 5. BRCA1 Influences Inflammatory Mechanisms in NP**

(A) Diagram of the experimental design.

(B–G) (B) Immunostaining of spinal microglia and NGF, (D) TNFα, and (F) TNFR1 in LV/sc + C286- and LV/BRCA1shRNA + C286treated rats (scale bars, 30 μm). Quantification of FI for (C) NGF, (E) TNFα, and (G) TNFR1. Data show Mean FI ± SEM, Student's t test, ***p ≤ 0.001 ($n$ = 3 per group, 5 sections per animal).

(Figures 4O and 4P). This effect was also seen for NGF, TNFα, and TNFR1 (Figures 5A–5G), indicating that an inflammatory environment was still present in the SC. Concurrent protein expression analysis of BDNF and the components of the MAPK and WNT pathways (FZD10 and Daxx), which had been modified by the agonist in L5-SNL non-transduced rats (see Figure 2), showed a significant increase with the suppression of BRCA1 despite the agonist treatment (Figures 6A–6H).

## DISCUSSION

Collectively, we show that C286 generates a "repair proficient" environment that may influence epigenetic modification of some enhancers in microglia, resetting the transcriptome toward a resting state after injury and thus reducing the long-term transcription of NP-associated genes. C286 modulates DNA repair mechanisms involving BRCA1 and ATM in spinal microglia, the former being directly linked to the P2XR4 phenotype and the development of NP. This supports the concept that transcription-induced persistent damage that is inefficiently repaired could chronically alter the epigenetic landscape, in line with the emerging importance of BRCA1 in neurodegenerative diseases (Mano et al., 2017; Suberbielle et al., 2015). Current therapeutic strategies generally aim at a single molecular target. These are yielding unsatisfactory results and are thus giving ground to a multifactorial

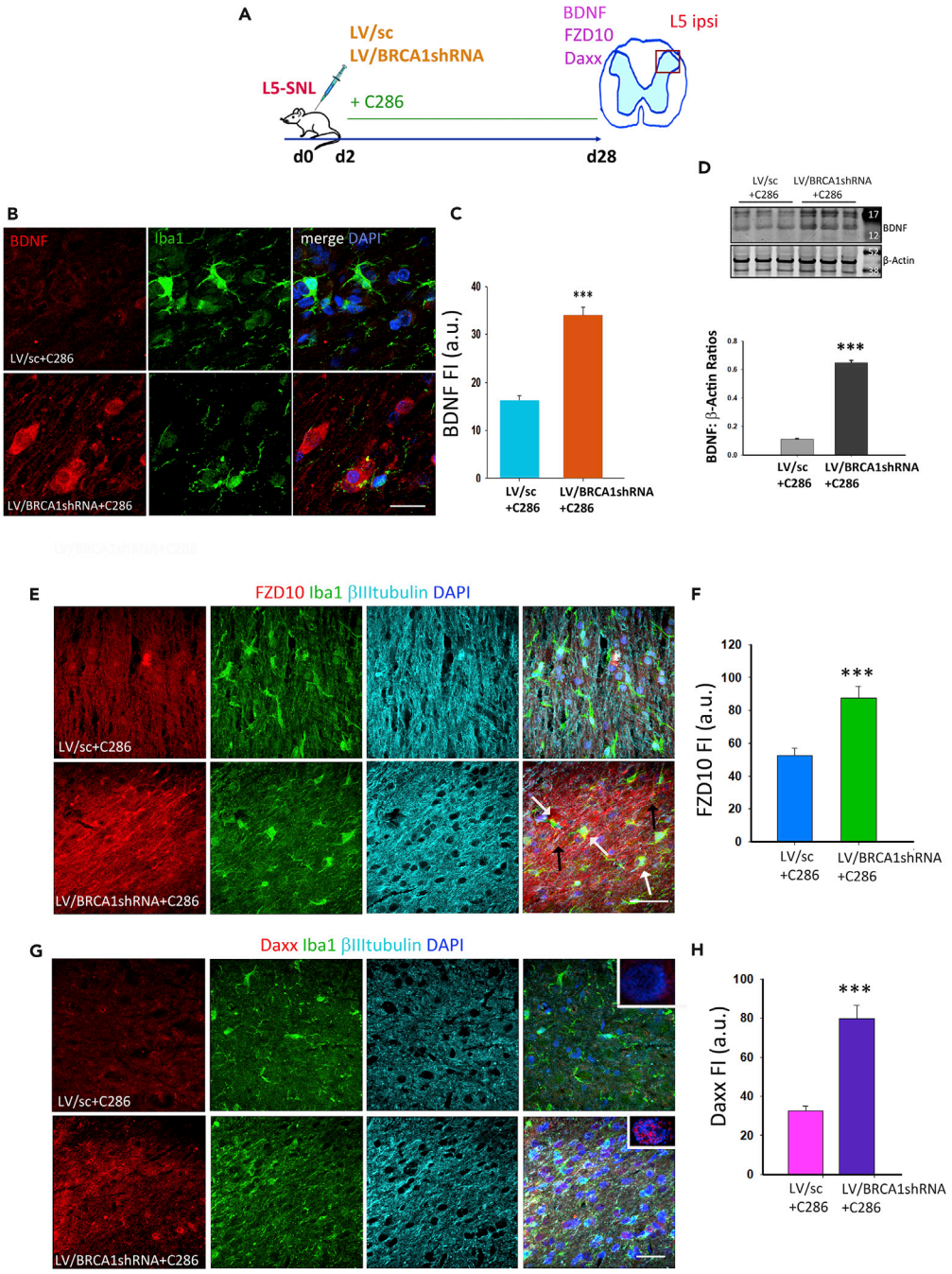


**Figure 6. BRCA1 Is Necessary for C286-Mediated Regulation of Pain**

(A) Diagram of the experimental design.

(B–D) (B and C) Immunostaining of spinal microglia for BDNF (scale bar, 50 μm) and its quantification. (D) Western blots of spinal cords for BDNF. Student's t test, n = 3 per group, ***p ≤ 0.001.

(E–H) (E and F) Expression and quantification of FZD10 (white arrows show colocalization with Iba1 and black arrows with βIII tubulin) and (G and H) Daxx in spinal neurons and microglia of LV/sc + C286- and LV/BRCA1shRNA + C286-treated rats (insets show its predominant nuclear localization). Scale bars, 100 μm for E and G. Data show Mean FI ± SEM, *n* = 3 per treatment group, 5 sections per animal. Student's t -test, **p ≤ 0.01, ***p ≤ 0.001.

approach targeting the numerous pathways involved, one possibility being to influence DNA repair mechanisms (Kelley and Fehrenbacher, 2017). Here we show that C286 has multiple effects on pathways that contribute to the chronicity of the neuronal sensitivity and thus might prove a more successful approach for the treatment of NP.

### RARβ Signaling and WNT/FZD Signaling

We found that the WNT pathway is one of the most significantly downregulated pathways by the agonist. The importance of the WNT/FZD signaling in signal transduction and synaptic plasticity alterations, which are essential to SC central sensitization after nerve injury, has been documented before (Zhang et al., 2013; Zhao and Yang, 2018). It is thought that WNT/FZD/β-catenin signaling contributes to the onset and persistence of pain after nerve injury, through activation of signaling pathways that recapitulate development, such as axon guidance, synaptic connection, and plasticity in the spinal cord. Spinal blockade of WNT signaling can inhibit the production and persistence of PNI-induced NP and prevent upregulation of the NR2B receptor and the subsequent $Ca^{2+}$-dependent signals CaMKII, Src/Tyr418, pPKCγ, ERK, and cAMP response element-binding protein within the SC pain pathways (Zhang et al., 2013). Curiously, we found that C286 suppresses WNT/FZD signaling and upregulates pathways involved in regeneration, which are also important during development. This may seem an incongruence, but we must consider that the overall biological effect is determined by a network of interacting pathways. WNT is known to interact with ephrinB-EphB receptor signaling, which also activates various developmental processes of the nervous system in response to nerve injury (Han et al., 2008; Song et al., 2008) and is thought to contribute to pain enhancement. These interactions may result in an exacerbation of neurochemical signs within development pathways that trigger and sustain pain pathways. Therefore, it is likely that the C286-mediated stimulation of the regeneration and development pathways is quite different, both qualitatively and quantitatively, because C286 upregulates transcription of these pathways to preinjury levels but not beyond. This promotes the restoration of homeostasis and prevents activation of pathways that sustain pain.

### RARβ and MAPK/Daxx Signaling

It is interesting that Daxx showed the highest downregulation within the MAPK pathway. Daxx is associated mostly with triggering apoptotic pathways that result in cell death and/or senescence. The agonist prevented the upregulation of Daxx in response to the injury and concomitantly upregulated various other pathways that are associated with normal cellular functions: cell-adhesion, mitochondria function, etc. The counterpart scenario, i.e., the downregulation of these pathways in the vehicle-treated rats, possibly reflects a state of compromised cellular functions in the SC. Therefore, it seems that Daxx could be an important contributor to cell fate in PNI-induced NP in the SC.

We found that RARβ activation downregulates TNF-α, which is one of the cytokines that induces phosphorylation and stabilization of Daxx through ASK1 activation. This is essential for activation of the pain signaling pathways, JNLK and p38 (Chang et al., 1998; Ichijo et al., 1997; Ji et al., 2009). Thus, it is possible that the marked downregulation of Daxx by C286 is in part a consequence of the agonist's anti-inflammatory effect. Similarly, the prevention of the reactive microglia P2X4R phenotype could be a direct consequence of a milder inflammatory milieu facilitated by the acute agonist action. Nonetheless, the overall effect of C286 cannot be justified entirely and solely by an initial anti-inflammatory effect. If that was the case, then anti-inflammatory treatment would be a successful therapeutic approach. Arguably, it is a combination of different mechanisms directly and indirectly affecting various intracellular functions: DNA repair, transcription, organelle transport, energy supply, and secretion of signaling molecules, which contributes to the RARβ modulation of NP.

### RARβ and the Extracellular Matrix

C286 also induced an upregulation of cell adhesion and cell junction pathways. This is noteworthy because adhesion proteins, which normally build and modify synapses, also participate in different aspects of synaptic and circuit reorganization associated with NP (Dina et al., 2004).

### C286 as a Promising Transcriptional Drug

We challenge the dogma that nuclear receptor agonists are unpromising therapeutic targets. Nuclear receptor signaling has been overlooked as a therapeutic avenue. Although nuclear receptor signaling regulates many pathways, it is thought that some of these might be detrimental to the cells casting

doubt on the overall biological effect. However, effective therapies need to be multifactorial, especially if they are aimed at chronic conditions in which a myriad of cellular functions has been altered. Retinoic acid modulates transcription and exerts its biological activity via the nuclear receptor RAR/RXR heterodimers, of which three isoforms have been identified (α,β,γ) (reviewed in Maden, 2007). Each isoform differs in spatial expression and yields different biological responses. In this regard, it is therefore beneficial to use specific receptor agonists targeted to the particular receptor that will induce the desired/anticipated effect. Because RXRs are promiscuous receptors and partner with various other nuclear receptors integrating their signaling pathways (Lefebvre et al., 2010), they are less attractive as drug targets. We have demonstrated target engagement previously and shown the upregulation of RARβ in response to treatment with specific RARβ agonists (Goncalves et al., 2018, 2019b). Our work illustrates an example of where a nuclear receptor agonist provides an effective treatment for a chronic condition without induction of detrimental pathways. C286 is currently undergoing a phase 1 trial (ISRCTN12424734) and can rapidly progress to further clinical testing proving an attractive therapeutic avenue to explore for NP.

### DNA Damage Pathways and Future Therapeutic Avenues

DNA damage has recently been proposed to play an important role in transcriptional regulation. Here we show that it is involved in setting an inflammatory state in spinal microglia that triggers NP. Our results demonstrate a novel role for BRCA1 in NP. BRCA1 is a DNA repair protein, best known for its association with breast cancer. We demonstrate that, by increasing DNA repair via BRCA1, NP can be prevented. This revolutionizes the therapeutic exploration for NP, shifting its focus from targets whose modification provides symptomatic and temporary amelioration to a more permanent disease-modifying target: DNA repair. Recovery of normal cellular functions through effective and timely DNA repair might be a successful prophylactic and/or therapeutic approach that is extendable to other chronic conditions similarly associated with an inflammatory etiology. Exploring other drugs that, like C286, modulate BRCA1 and identifying other key DNA repair mechanisms could be a step change in therapeutic development.

### Limitations of the Study

This study was conducted in male rats only and as such does not address the sexual dimorphism in pain.

## METHODS

All methods can be found in the accompanying Transparent Methods supplemental file.

## SUPPLEMENTAL INFORMATION

Supplemental Information can be found online at https://doi.org/10.1016/j.isci.2019.09.020.

## ACKNOWLEDGMENTS

This work was funded by the Wellcome Trust (Grant ref. no 084286) to J.P.T.C., Wellcome Trust (Grant ref. no 110047/Z/15/Z) to A.M.C., MRC (Grant ref. no MR/R006466/1) to J.P.T.C. and M.B.G., and Genopole Thematic Incentive Actions funding (ATIGE-2017) and the institutional bodies CEA, CNRS, and Université d'Evry-Val d'Essonne to J.M. and M.A.M.-P.

## AUTHOR CONTRIBUTIONS

M.B.G., J.P.T.C., and M.A.M.-P. conceived and designed the study. M.B.G. wrote the paper. M.B.G., E.C., J.G., C.H., J.M., and M.A.M.-P. performed the experiments and analyzed the data. J.M. and M.A.M.-P. prepared the Supplemental Information. All authors discussed the results and commented on the manuscript.

## DECLARATION OF INTERESTS

The authors declare no competing financial interests. C286 synthesis and use in nerve injuries and neuropathic pain is protected under patents (PCT/EP2015/08,002; PCT/EP2017/0604802; GB1907647).

Received: June 13, 2019
Revised: August 6, 2019
Accepted: September 12, 2019
Published: October 25, 2019

## REFERENCES

Alt, F.W., and Schwer, B. (2018). DNA double-strand breaks as drivers of neural genomic change, function, and disease. DNA Repair (Amst.) *71*, 158–163.

Amaya, F., Izumi, Y., Matsuda, M., and Sasaki, M. (2013). Tissue injury and related mediators of pain exacerbation. Curr. Neuropharmacol. *11*, 592–597.

Bajpe, P.K., Heynen, G.J., Mittempergher, L., Grernrum, W., de Rink, I.A., Nijkamp, W., Beijersbergen, R.L., Bernards, R., and Huang, S. (2013). The corepressor CTBP2 is a coactivator of retinoic acid receptor/retinoid X receptor in retinoic acid signaling. Mol. Cell. Biol. *33*, 3343–3353.

Bar-Shira, A., Rashi-Elkeles, S., Zlochover, L., Moyal, L., Smorodinsky, N.I., Seger, R., and Shiloh, Y. (2002). ATM-dependent activation of the gene encoding MAP kinase phosphatase 5 by radiomimetic DNA damage. Oncogene *21*, 849–855.

Beggs, S., Trang, T., and Salter, M.W. (2012). P2X4R+ microglia drive neuropathic pain. Nat. Neurosci. *15*, 1068–1073.

Borsook, D., Hargreaves, R., Bountra, C., and Porreca, F. (2014). Lost but making progress–Where will new analgesic drugs come from? Sci. Transl. Med. *6*, 249sr243.

Calvo, M., Zhu, N., Grist, J., Ma, Z., Loeb, J.A., and Bennett, D.L. (2011). Following nerve injury neuregulin-1 drives microglial proliferation and neuropathic pain via the MEK/ERK pathway. Glia *59*, 554–568.

Chang, H.Y., Nishitoh, H., Yang, X., Ichijo, H., and Baltimore, D. (1998). Activation of apoptosis signal-regulating kinase 1 (ASK1) by the adapter protein Daxx. Science *281*, 1860–1863.

de Jager, C.A., Oulhaj, A., Jacoby, R., Refsum, H., and Smith, A.D. (2011). Cognitive and clinical outcomes of homocysteine-lowering B-vitamin treatment in mild cognitive impairment: a randomized controlled trial. Int. J. Geriatr. Psychiatry *27*, 592–600.

Denk, F., Crow, M., Didangelos, A., Lopes, D.M., and McMahon, S.B. (2016). Persistent alterations in microglial enhancers in a model of chronic pain. Cell Rep. *15*, 1771–1781.

Descalzi, G., Ikegami, D., Ushijima, T., Nestler, E.J., Zachariou, V., and Narita, M. (2015). Epigenetic mechanisms of chronic pain. Trends Neurosci. *38*, 237–246.

Dheen, S.T., Jun, Y., Yan, Z., Tay, S.S., and Ling, E.A. (2005). Retinoic acid inhibits expression of TNF-alpha and iNOS in activated rat microglia. Glia *50*, 21–31.

Di, L.J., Fernandez, A.G., De Siervi, A., Longo, D.L., and Gardner, K. (2010). Transcriptional regulation of BRCA1 expression by a metabolic switch. Nat. Struct. Mol. Biol. *17*, 1406–1413.

Dina, O.A., Parada, C.A., Yeh, J., Chen, X., McCarter, G.C., and Levine, J.D. (2004). Integrin signaling in inflammatory and neuropathic pain in the rat. Eur. J. Neurosci. *19*, 634–642.

Edelmayer, R.M., Brederson, J.D., Jarvis, M.F., and Bitner, R.S. (2014). Biochemical and pharmacological assessment of MAP-kinase signaling along pain pathways in experimental rodent models: a potential tool for the discovery of novel antinociceptive therapeutics. Biochem. Pharmacol. *87*, 390–398.

Ellis, A., and Bennett, D.L. (2013). Neuroinflammation and the generation of neuropathic pain. Br. J. Anaesth. *111*, 26–37.

Fernandes, N.D., Sun, Y., and Price, B.D. (2007). Activation of the kinase activity of ATM by retinoic acid is required for CREB-dependent differentiation of neuroblastoma cells. J. Biol. Chem. *282*, 16577–16584.

Fong, Y.W., Cattoglio, C., and Tjian, R. (2013). The intertwined roles of transcription and repair proteins. Mol. Cell *52*, 291–302.

Gardini, A., Baillat, D., Cesaroni, M., and Shiekhattar, R. (2014). Genome-wide analysis reveals a role for BRCA1 and PALB2 in transcriptional co-activation. EMBO J. *33*, 890–905.

Gereau, R.W.t., Sluka, K.A., Maixner, W., Savage, S.R., Price, T.J., Murinson, B.B., Sullivan, M.D., and Fillingim, R.B. (2014). A pain research agenda for the 21st century. J. Pain *15*, 1203–1214.

Goncalves, M.B., Malmqvist, T., Clarke, E., Hubens, C.J., Grist, J., Hobbs, C., Trigo, D., Risling, M., Angeria, M., Damberg, P., et al. (2015). Neuronal RARbeta signaling modulates pten activity directly in neurons and via exosome transfer in astrocytes to prevent glial scar formation and induce spinal cord regeneration. J. Neurosci. *35*, 15731–15745.

Goncalves, M.B., Clarke, E., Jarvis, C.I., Barret Kalindjian, S., Pitcher, T., Grist, J., Hobbs, C., Carlstedt, T., Jack, J., Brown, J.T., et al. (2019a). Discovery and lead optimisation of a potent, selective and orally bioavailable RARbeta agonist for the potential treatment of nerve injury. Bioorg. Med. Chem. Lett. *29*, 995–1000.

Goncalves, M.B., Wu, Y., Clarke, E., Grist, J., Hobbs, C., Trigo, D., Jack, J., and Corcoran, J.P.T. (2019b). Regulation of myelination by exosome associated retinoic acid release from NG2-positive cells. J. Neurosci. *39*, 3013–3027.

Goncalves, M.B., Wu, Y., Trigo, D., Clarke, E., Malmqvist, T., Grist, J., Hobbs, C., Carlstedt, T.P., and Corcoran, J.P.T. (2018). Retinoic acid synthesis by NG2 expressing cells promotes a permissive environment for axonal outgrowth. Neurobiol. Dis. *111*, 70–79.

Han, Y., Song, X.S., Liu, W.T., Henkemeyer, M., and Song, X.J. (2008). Targeted mutation of EphB1 receptor prevents development of neuropathic hyperalgesia and physical dependence on morphine in mice. Mol. Pain *4*, 60.

Hu, C., Liu, J., Zhang, Y., Li, Y., Xie, W., and Zhao, C. (2009). A useful transgenic mouse line for studying the development of spinal nociceptive circuits. Neurosci. Lett. *450*, 211–216.

Hur, E.M., Saijilafu, and Zhou, F.Q. (2012). Growing the growth cone: remodeling the cytoskeleton to promote axon regeneration. Trends Neurosci. *35*, 164–174.

Ichijo, H., Nishida, E., Irie, K., ten Dijke, P., Saitoh, M., Moriguchi, T., Takagi, M., Matsumoto, K., Miyazono, K., and Gotoh, Y. (1997). Induction of apoptosis by ASK1, a mammalian MAPKKK that activates SAPK/JNK and p38 signaling pathways. Science *275*, 90–94.

Iyengar, S., Ossipov, M.H., and Johnson, K.W. (2017). The role of calcitonin gene-related peptide in peripheral and central pain mechanisms including migraine. Pain *158*, 543–559.

Jensen, T.S., and Finnerup, N.B. (2014). Allodynia and hyperalgesia in neuropathic pain: clinical manifestations and mechanisms. Lancet Neurol. *13*, 924–935.

Ji, R.R., Baba, H., Brenner, G.J., and Woolf, C.J. (1999). Nociceptive-specific activation of ERK in spinal neurons contributes to pain hypersensitivity. Nat. Neurosci. *2*, 1114–1119.

Ji, R.R., Gereau, R.W.t., Malcangio, M., and Strichartz, G.R. (2009). MAP kinase and pain. Brain Res. Rev. *60*, 135–148.

Jiang, Q., Lee, C.Y., Mandrekar, S., Wilkinson, B., Cramer, P., Zelcer, N., Mann, K., Lamb, B., Willson, T.M., Collins, J.L., et al. (2008). ApoE promotes the proteolytic degradation of Abeta. Neuron *58*, 681–693.

Jin, S.X., Zhuang, Z.Y., Woolf, C.J., and Ji, R.R. (2003). p38 mitogen-activated protein kinase is activated after a spinal nerve ligation in spinal cord microglia and dorsal root ganglion neurons and contributes to the generation of neuropathic pain. J. Neurosci. *23*, 4017–4022.

Kawasaki, Y., Kohno, T., Zhuang, Z.Y., Brenner, G.J., Wang, H., Van Der Meer, C., Befort, K., Woolf, C.J., and Ji, R.R. (2004). Ionotropic and metabotropic receptors, protein kinase A, protein kinase C, and Src contribute to C-fiber-induced ERK activation and cAMP response element-binding protein phosphorylation in dorsal horn neurons, leading to central sensitization. J. Neurosci. *24*, 8310–8321.

Kelley, M.R., and Fehrenbacher, J.C. (2017). Challenges and opportunities identifying therapeutic targets for chemotherapy-induced peripheral neuropathy resulting from oxidative DNA damage. Neural Regen. Res. *12*, 72–74.

Kim, S.H., and Chung, J.M. (1992). An experimental model for peripheral neuropathy produced by segmental spinal nerve ligation in the rat. Pain *50*, 355–363.

Lefebvre, P., Benomar, Y., and Staels, B. (2010). Retinoid X receptors: common heterodimerization partners with distinct functions. Trends Endocrinol. Metab. *21*, 676–683.

Lindsay, C.R., Morozov, V.M., and Ishov, A.M. (2008). PML NBs (ND10) and Daxx: from nuclear structure to protein function. Front. Biosci. *13*, 7132–7142.

Madabhushi, R., Gao, F., Pfenning, A.R., Pan, L., Yamakawa, S., Seo, J., Rueda, R., Phan, T.X.,

Yamakawa, H., Pao, P.C., et al. (2015). Activity-induced DNA breaks govern the expression of neuronal early-response genes. Cell *161*, 1592–1605.

Maden, M. (2007). Retinoic acid in the development, regeneration and maintenance of the nervous system. Nat. Rev. Neurosci. *8*, 755–765.

Mano, T., Nagata, K., Nonaka, T., Tarutani, A., Imamura, T., Hashimoto, T., Bannai, T., Koshi-Mano, K., Tsuchida, T., Ohtomo, R., et al. (2017). Neuron-specific methylome analysis reveals epigenetic regulation and tau-related dysfunction of BRCA1 in Alzheimer's disease. Proc. Natl. Acad. Sci. U S A *114*, E9645–E9654.

Mapplebeck, J.C.S., Dalgarno, R., Tu, Y., Moriarty, O., Beggs, S., Kwok, C.H.T., Halievski, K., Assi, S., Mogil, J.S., Trang, T., et al. (2018). Microglial P2X4R-evoked pain hypersensitivity is sexually dimorphic in rats. Pain *159*, 1752–1763.

Marnef, A., Cohen, S., and Legube, G. (2017). Transcription-coupled DNA double-strand break repair: active genes need special care. J. Mol. Biol. *429*, 1277–1288.

McDonald, M.K., Tian, Y., Qureshi, R.A., Gormley, M., Ertel, A., Gao, R., Aradillas Lopez, E., Alexander, G.M., Sacan, A., Fortina, P., et al. (2014). Functional significance of macrophage-derived exosomes in inflammation and pain. Pain *155*, 1527–1539.

Meacham, K., Shepherd, A., Mohapatra, D.P., and Haroutounian, S. (2017). Neuropathic pain: central vs. peripheral mechanisms. Curr. Pain Headache Rep. *21*, 28.

Moran, M.M., and Szallasi, A. (2018). Targeting nociceptive transient receptor potential channels to treat chronic pain: current state of the field. Br. J. Pharmacol. *175*, 2185–2203.

Noristani, H.N., Gerber, Y.N., Sabourin, J.C., Le Corre, M., Lonjon, N., Mestre-Frances, N., Hirbec, H.E., and Perrin, F.E. (2017). RNA-seq analysis of microglia reveals time-dependent activation of specific genetic programs following spinal cord injury. Front. Mol. Neurosci. *10*, 90.

Obata, K., and Noguchi, K. (2004). MAPK activation in nociceptive neurons and pain hypersensitivity. Life Sci. *74*, 2643–2653.

Patil, S.B., Brock, J.H., Colman, D.R., and Huntley, G.W. (2011). Neuropathic pain- and glial derived neurotrophic factor-associated regulation of cadherins in spinal circuits of the dorsal horn. Pain *152*, 924–935.

Puc, J., Aggarwal, A.K., and Rosenfeld, M.G. (2017). Physiological functions of programmed DNA breaks in signal-induced transcription. Nat. Rev. Mol. Cell Biol. *18*, 471–476.

Rhinn, M., and Dolle, P. (2012). Retinoic acid signalling during development. Development *139*, 843–858.

Roubert, A., Gregory, K., Li, Y., Pfalzer, A.C., Li, J., Schneider, S.S., Wood, R.J., and Liu, Z. (2017). The influence of tumor necrosis factor-alpha on the tumorigenic Wnt-signaling pathway in human mammary tissue from obese women. Oncotarget *8*, 36127–36136.

Ruscheweyh, R., Wilder-Smith, O., Drdla, R., Liu, X.G., and Sandkuhler, J. (2011). Long-term potentiation in spinal nociceptive pathways as a novel target for pain therapy. Mol. Pain *7*, 20.

Sharma, A., Singh, K., and Almasan, A. (2012). Histone H2AX phosphorylation: a marker for DNA damage. Methods Mol. Biol. *920*, 613–626.

Sharma, N., Gabel, H.W., and Greenberg, M.E. (2015). A shortcut to activity-dependent transcription. Cell *161*, 1496–1498.

Shiue, S.J., Rau, R.H., Shiue, H.S., Hung, Y.W., Li, Z.X., Yang, K.D., and Cheng, J.K. (2019). Mesenchymal stem cell exosomes as a cell-free therapy for nerve injury-induced pain in rats. Pain *160*, 210–223.

Song, X.J., Cao, J.L., Li, H.C., Zheng, J.H., Song, X.S., and Xiong, L.Z. (2008). Upregulation and redistribution of ephrinB and EphB receptor in dorsal root ganglion and spinal dorsal horn neurons after peripheral nerve injury and dorsal rhizotomy. Eur. J. Pain *12*, 1031–1039.

Song, X.S., Cao, J.L., Xu, Y.B., He, J.H., Zhang, L.C., and Zeng, Y.M. (2005). Activation of ERK/CREB pathway in spinal cord contributes to chronic constrictive injury-induced neuropathic pain in rats. Acta Pharmacol. Sin. *26*, 789–798.

Su, Y., Ming, G.L., and Song, H. (2015). DNA damage and repair regulate neuronal gene expression. Cell Res. *25*, 993–994.

Suberbielle, E., Djukic, B., Evans, M., Kim, D.H., Taneja, P., Wang, X., Finucane, M., Knox, J., Ho, K., Devidze, N., et al. (2015). DNA repair factor BRCA1 depletion occurs in Alzheimer brains and impairs cognitive function in mice. Nat. Commun. *6*, 8897.

Takahashi, Y., Lallemand-Breitenbach, V., Zhu, J., and de The, H. (2004). PML nuclear bodies and apoptosis. Oncogene *23*, 2819–2824.

Tang, S.J. (2014). Synaptic activity-regulated Wnt signaling in synaptic plasticity, glial function and chronic pain. CNS Neurol. Disord. Drug Targets *13*, 737–744.

Ulmann, L., Levavasseur, F., Avignone, E., Peyroutou, R., Hirbec, H., Audinat, E., and Rassendren, F. (2013). Involvement of P2X4 receptors in hippocampal microglial activation after status epilepticus. Glia *61*, 1306–1319.

Wahezi, S.E., Silva, K., and Najafi, S. (2015). Pain relief with percutaneous trochanteroplasty in a patient with bilateral trochanteric myelomatous lytic lesions. Pain Physician *18*, E57–E63.

Wu, A., Green, C.R., Rupenthal, I.D., and Moalem-Taylor, G. (2012). Role of gap junctions in chronic pain. J. Neurosci. Res. *90*, 337–345.

Zhang, G., and Yang, P. (2017). Bioinformatics genes and pathway analysis for chronic neuropathic pain after spinal cord injury. Biomed. Res. Int. *2017*, 6423021.

Zhang, Y.K., Huang, Z.J., Liu, S., Liu, Y.P., Song, A.A., and Song, X.J. (2013). WNT signaling underlies the pathogenesis of neuropathic pain in rodents. J. Clin. Invest. *123*, 2268–2286.

Zhao, Y., and Yang, Z. (2018). Effect of Wnt signaling pathway on pathogenesis and intervention of neuropathic pain. Exp. Ther. Med. *16*, 3082–3088.

**ISCI, Volume *20***

## Supplemental Information

# RARβ Agonist Drug (C286) Demonstrates Efficacy in a Pre-clinical Neuropathic Pain Model Restoring Multiple Pathways via DNA Repair Mechanisms

**Maria B. Goncalves, Julien Moehlin, Earl Clarke, John Grist, Carl Hobbs, Antony M. Carr, Julian Jack, Marco Antonio Mendoza-Parra, and Jonathan P.T. Corcoran**

A

| | Number of reads before alignment | Number of reads after alignment | Percentage of reads aligned |
|---|---|---|---|
| JC12 | 24 513 566 | 20 107 168 | 82.03% |
| JC13 | 27 181 807 | 21 410 429 | 78.76% |
| JC16 | 27 095 268 | 20 872 629 | 76.99% |
| JC17 | 28 078 948 | 22 811 788 | 77.76% |
| JC18 | 23 885 123 | 19 134 372 | 80.11% |
| JC48 | 23 770 228 | 19 318 864 | 81.27% |
| JC49 | 26 164 534 | 21 156 238 | 80.86% |
| JC50 | 24 076 835 | 19 519 668 | 81.07% |
| JC51 | 27 750 882 | 22 770 701 | 82.05% |
| JC52 | 27 405 453 | 22 280 331 | 81.31% |
| JC53 | 25 458 422 | 20 692 977 | 81.17% |

B

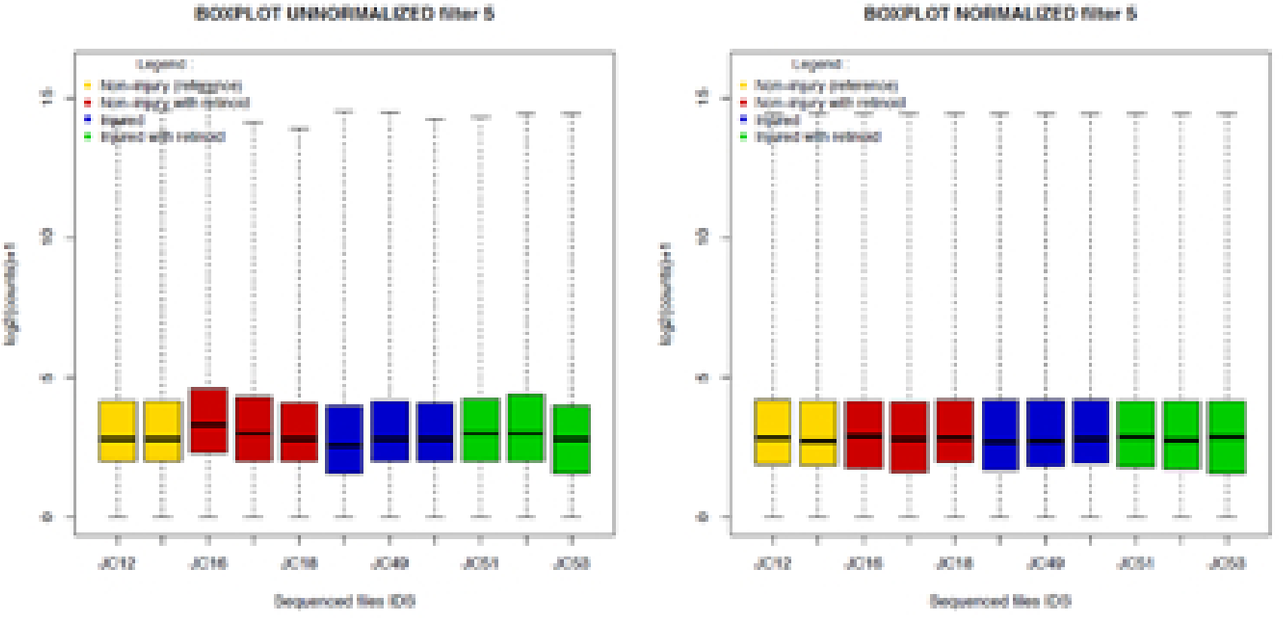


C

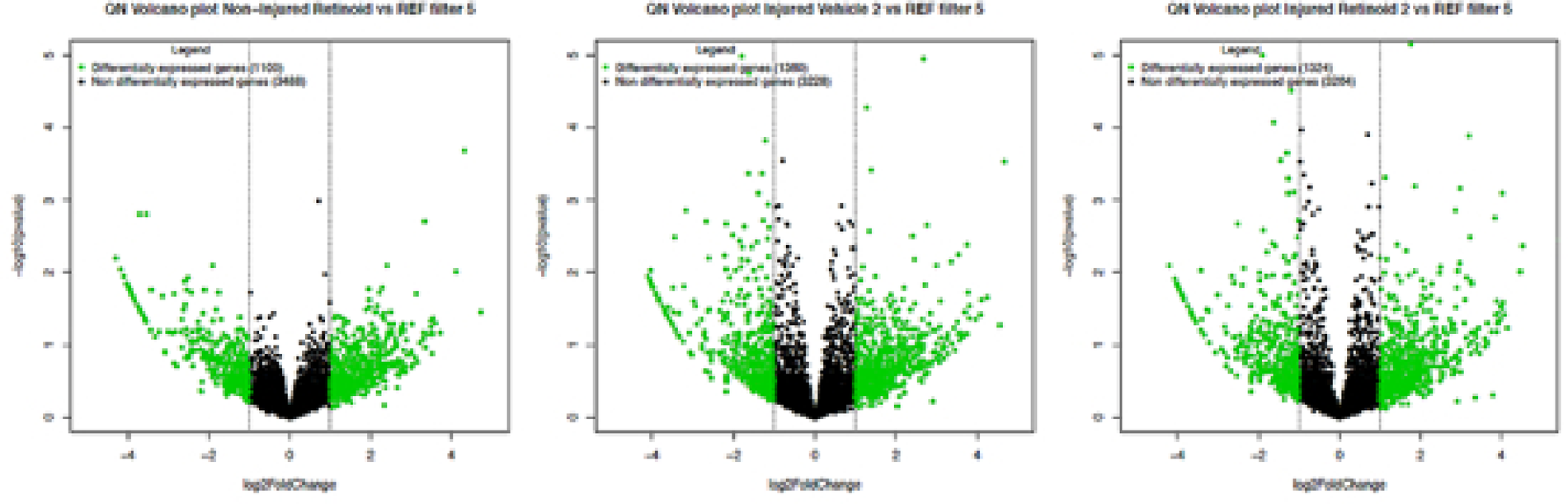

# Co-expresion path 1

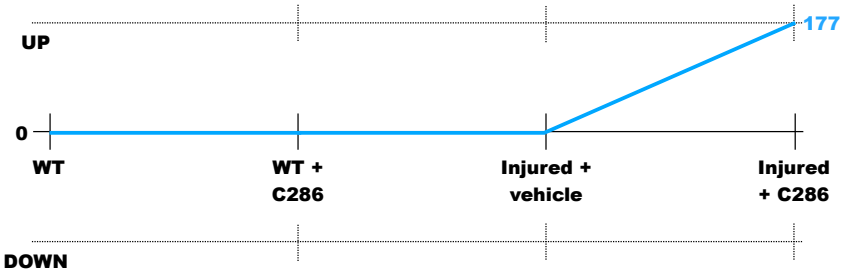


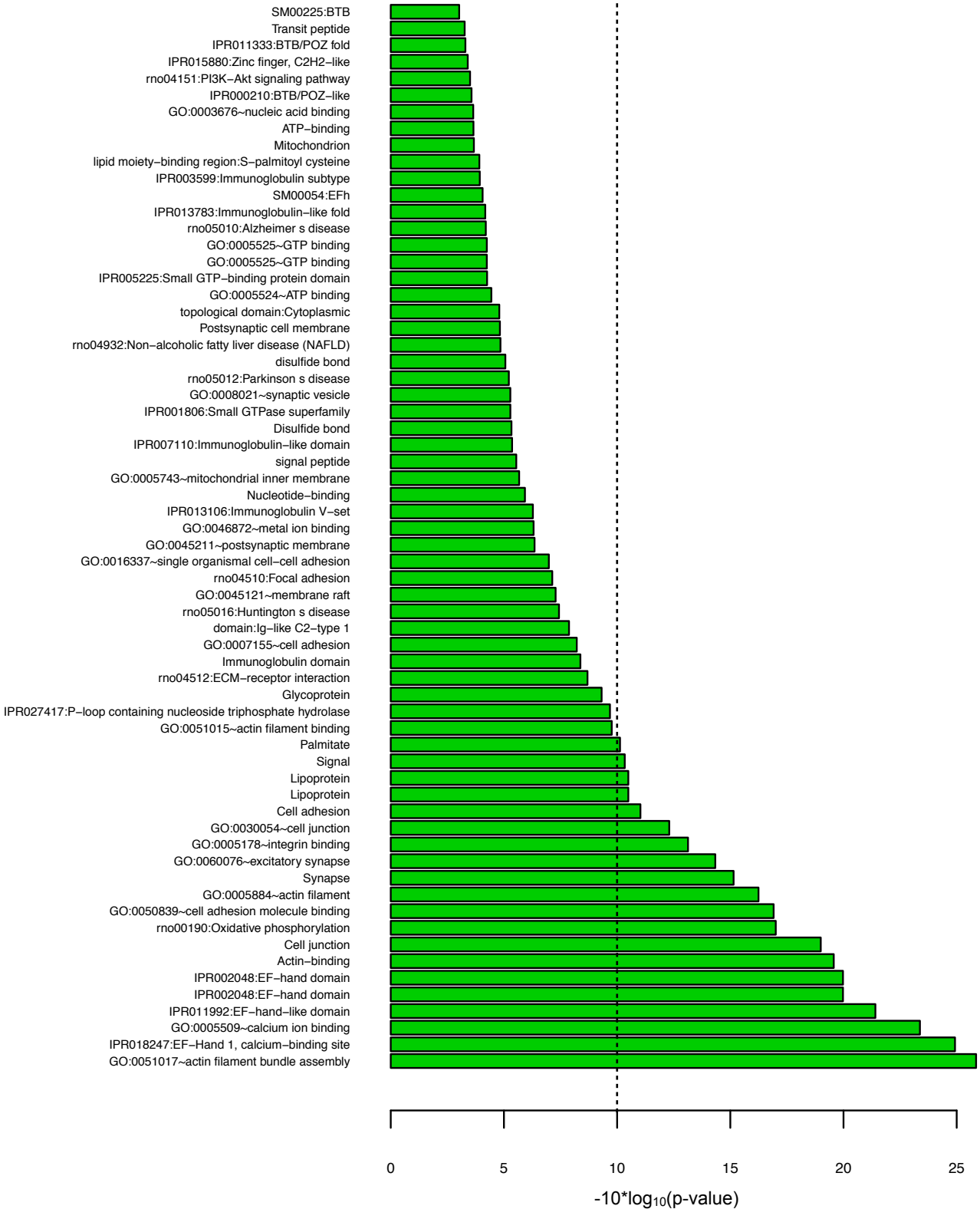

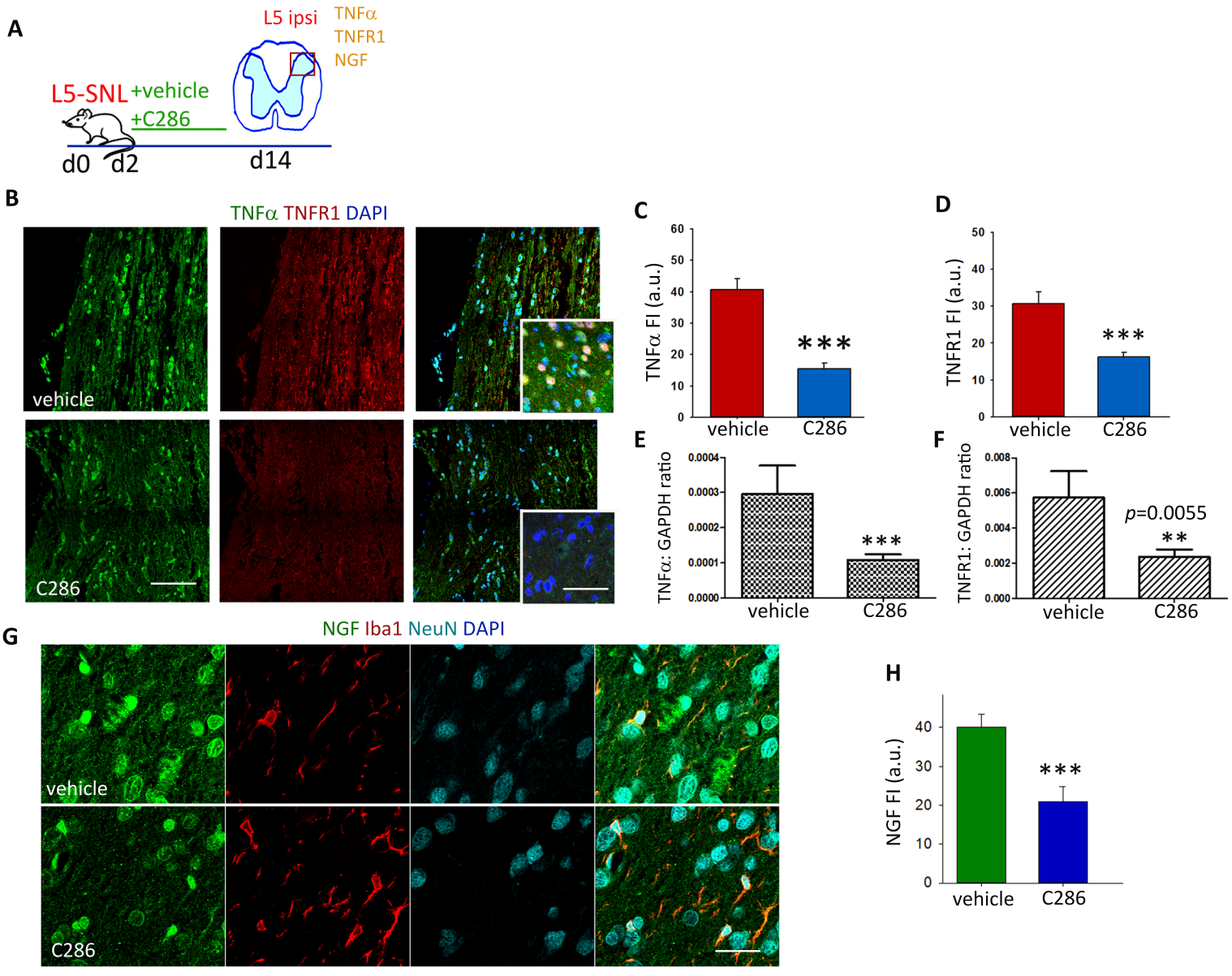
A
L5 ipsi
TNFα
TNFR1
NGF
L5-SNL
+vehicle
+C286
d0
d2
d14
B
TNFα TNFR1 DAPI
vehicle
C286
C
TNFα FI (a.u.)
***
vehicle
C286
D
TNFR1 FI (a.u.)
***
vehicle
C286
E
TNFα: GAPDH ratio
***
vehicle
C286
F
TNFR1: GAPDH ratio
p=0.0055
**
vehicle
C286
G
NGF Iba1 NeuN DAPI
vehicle
C286
H
NGF FI (a.u.)
***
vehicle
C286

**Figure S1. Transcriptomics analysis of spinal cord samples issued from animals under different conditions**

**A,** Summary of the number of DNA sequenced reads obtained per sample as well as the fraction retained after alignment to the Rattus norvegicus reference Genome. **B,** Boxplots depicting the read counts per gene prior or after quantile normalization. **C**, Volcano plot illustrating the fraction of differentially expressed genes (rel. to non-injured + vehicle condition), as defined by a two-fold change criterion, and their related confidence (p-value).

**Figure S2. Gene Ontology (GO) enrichment analysis on co-expressed genes (http://dx.doi.org/10.17632/kjvs5vgkbf.1DOI)**

Considering 3 differentially expressed conditions (non-injured + C286; injured + vehicle; injured + C286) and three gene expression states (induced, repressed and non-differentially expressed), a total of 26 combinatorial gene co-expression events are theoretically possible. Genes were classified on the basis of their co-expression behavior over the various conditions**.** GO terms associated to the co-expressed genes are displayed on the basis of their confidence ($-10*\log_{10}$(p-value), as inferred by the DAVID bioinformatics resources (Huang da et al., 2009). Co-expression path 1 is shown here, all the other paths are available in **(http://dx.doi.org/10.17632/kjvs5vgkbf.1DOI).**

**Figure S3. Modulation of TNFα, TNFR1 and NGF by C286**

**a**, Diagram of the experimental design. **b-d,** Immunostaining and quantification of TNFα and TNFR1 by IF (scale bars are 100μm and 50 μm for insets) and by **e,f,** RT-qPCR. Student's *t*-test, $^{**}p \leq 0.01$, $^{***}p \leq 0.001$, ($n$= 3 per group). **g,** NGF expression in spinal neurons and microglia (scale bar is 30μm) and **h**, quantification of total FI. Data shows Mean FI ± SEM. Student's *t*-test, $^{**}p \leq 0.01$, $^{***}p \leq 0.001$, ($n$= 3 per group, 5 sections per animal).

**Table S1. Summary of the GO terms for all 20 co-expression paths (http://dx.doi.org/10.17632/kjvs5vgkbf.1DOI)**

The p-value is expressed in "-10*log10(p-value)" and for each path it is indicated their corresponding status (i.e. [0][1][0] indicated the expression status for [Non-Injured+C286][Injured+Veh][Injured+C286]).

## Transparent Methods

### Rats and animal procedures

All procedures were in accordance with the UK Home Office guidelines and Animals (Scientific Procedures) Act of 1986. Male Sprague Dawleys rats, weighing 220-250 grams were used throughout the study. All animal care and experimental procedures complied with the Animals (Scientific Procedures) Act, 1986 of the UK Parliament, Directive 2010/63/EU of the European Parliament and the Guide for the Care and Use of Laboratory Animals published by the US National Institutes of Health (NIH Publication No. 85–23, revised 1996). Animal studies are reported in compliance with the ARRIVE guidelines (Kilkenny et al., 2010; McGrath and Lilley, 2015). All surgery, behavioural testing and analyses were performed using a randomized block design and in a blinded fashion. Allocation concealment was performed by having the treatment stocks coded by a person independent of the study. Codes were only broken after the end of the study.

Animals were housed in groups of three to four in Plexiglas cages with tunnels and bedding, on a 12:12 h light/dark cycle and had access to food and water ad libitum. Experimental neuropathy was induced by an L5 spinal nerve ligation (Bennett et al., 2003) (L5 SNL-2 week analysis; *n*= 6 per treatment group; L5 SNL- 4 week analysis *n*= 8 per treatment group; L5 SNL with lentivirus; n=6 per treatment group)**.** Briefly, rats were anesthetized via intraperitoneal injection of 0.25 mg $kg^{-1}$ medetomidine/60 mg $kg^{-1}$ ketamine solution, following which the vertebral transverse processes were exposed via a small skin incision and

retraction of the paravertebral musculature. The L6 transverse process was partially removed and the L5 spinal nerve was identified, tightly ligated, and sectioned 1–2 mm distal to the silk ligature. During the surgery, the rats were placed on a controlled heating pad to maintain temperature at 37 ± 1°C. After the surgery, the rats were hydrated with physiological saline (2 mL, s.c.). Anesthesia was reversed with an intra muscular (IM) injection of 0.05 ml (1 mg/kg) atipamezole hydrochloride (Antisedan®; Pfizer Animal Health, Exton, PA). Animals were kept in a heated recovery box until fully conscious and analgesia (buprenorphine, 0.01 mg/ kg, subcutaneously) was given after suturing and recovery. All the rats survived this surgery.

For BRCA1 loss of function studies, at the time of the L5 SNL, 5 µl of lentivirus (titer: $3.67 \times 10^8$ TU/ml), either Brca1 Rat shRNA Lentiviral Particle, sequence, TACACAGCCTGGTGTCTCTAAGCAGAGTG, or scrambled, sequence, GCACTACCAGAGCTAACTCAGATAGTACT (TL709162V, Origene**)** was injected manually into the spinal cord at the level of L5, using a 20 µl Hamilton syringe at 0.5 µl $min^{-1}$ and the needle was left in place for the following 5 minutes to limit diffusion through the needle tract.

**Drug treatments and tissue processing for in vivo studies**

Rats were treated with vehicle or a novel selective RARβ agonist, C286 (Goncalves et al., 2019a) (synthesized by Sygnature Chemical Services, Nottingham, UK), given by oral gavage (po) three times a week for four weeks at 3mg/kg. C286 has a high potency at RARβ (similar potency to all-trans-retinoic acid) and behaves as a full agonist showing an $EC_{50}$ of 1.94 nM at the mouse RARβ receptor and a selectivity for RARβ over RARα of 13.4, with selectivity for RARβ over RARγ being 5.6-fold (Goncalves et al., 2019a).

After defined survival times, animals were killed by terminal anesthetization and transcardially perfused with 4% paraformaldehyde, for immunohistochemistry or ice-cold PBS, for mRNA

extraction and Western blotting. The lumbar spinal cords were excised, rapidly removed and the tissue corresponding to L5 spinal cord was isolated. For immunohistochemistry, the tissue was post-fixed with 4% PFA for at least two days at room temperature before being embedded in paraffin wax. Five μm longitudinal or transverse sections cut throughout each block. Sets of consecutive sections, comprising the L5 lumbar spinal cord were taken and used for immunohistochemical analysis. For mRNA extraction and Western blotting, L5 spinal cords were bi-dissected into ipsi and contralateral side to the injury, and tissue was snap frozen in liquid nitrogen and kept at -80 $^{0}$C until further use.

**Behavioural tests**

Pain thresholds were measured according to the methods described below. Baseline recordings were taken at 1 day prior to surgery and at 1, 6, 9, 16, 23 and 28 days after surgery for L5 SNL experiment and at 1, 7, 14, 21 and 28 days for the L5 SNL lentivirus study.

**Mechanical thresholds**

**von Frey test**

Static mechanical withdrawal thresholds were assessed by applying von Frey hairs (Touch Test, Stoelting, IL, USA) to the plantar surface of the hind paw. Unrestrained animals were acclimatised in acrylic cubicles (8 x 5x 10 cm) on a wire mesh grid for 60 min prior to testing. Calibrated von Frey hairs (flexible nylon fibres of increasing diameter that exert defined levels of force) were applied to the plantar surface of the hind paw until the fibre bent. The hair was held in place for 3 secs or until the paw was withdrawn in a reflex not associated with movement or grooming. Each hair was applied 5 times to both the left and the right paw alternately, starting with the lowest force hair. Hairs of increasing force were applied in

sequence, 5 applications per hair. A positive response was recorded when a 40% withdrawal response occurred over 5 applications.

**Randall-Selitto test**

Mechanical nociceptive thresholds were evaluated using an Analgesy-Meter (Ugo Basile, Comerio, Italy). Rats were gently held and incremental pressure (maximum 25 g) was applied onto the dorsal surface of the hind paw. The pressure required to elicit paw withdrawal, the paw pressure threshold, in g was determined. An average of three recordings were taken separated by at least 5 minutes.

**Thermal thresholds**

**Hot plate- Hargreaves test**

Briefly, the rats were habituated for 10 minutes to an apparatus consisting of individual Plexiglas boxes on an elevated glass table. A mobile radiant heat source was located under the table and focused on the hind paw, and the paw withdrawal latencies were defined as the time taken by the rat to remove its hind paw from the heat source. The cut-off point was set at 25 s to prevent tissue damage. The apparatus was calibrated to give a paw withdrawal latency of approximately 15 s in naïve rats. An average of three recordings were taken separated by at least 5 minutes.

**Cold plate**

Withdrawal of the hind paw in response to painful cold stimulation was assessed using an Incremental Hot/Cold Plate (IITC Life Sciences) set at 4±0.1°C. Rats were lightly restrained and the hind paw was held with the plantar surface on the cold plate. The latency to withdraw the paw was measured to the nearest 0.01secs. To avoid tissue injury, the maximum latency

period permitted was 20 secs. An average of three recordings were taken separated by at least 5 minutes.

**RNA extraction and Sequencing**

**Total RNA isolation and RT-qPCR analysis**

Frozen micro dissected spinal cord samples were lysed with Teflon-glass homogenisers and QIAshredder columns (Qiagen). Total RNA was isolated with the Qiagen RNeasy® Mini kit. The RNA was assessed for purity and quantity using the Nanodrop 1000 spectrophotometer and assessed for quality on the Agilent Bioanalyzer 2100. RNA was reverse transcribed with a QuantiTect® Reverse Transcription kit (Qiagen). Levels of BRCA1, TNFα and TNFR1 expression were quantitated in triplicate, relative to GAPDH and triplicate non-template controls for each gene, by RT-qPCR analysis on a LightCycler® 480 instrument with LightCycler® SYBR® Green I Master reagent (Roche). Primer pairs used were; BRCA1 F: 5'-AGGCAAGATCTCGAAGGAACCC-3'; R: 5'-AATCAGGGTCTCTGCTGGAGACTA-3'; TNFα F: 5'-CTGTGCCTCAGCCTCTTCTC-3'; R: 5'-ACTGATGAGAGGGAGCCCAT-3'; TNFR1 F: 5'-CCTCTCTCCCCTCGGCTTTA-3'; R: 5'-CCCGGGTTAGAAAGGCTCAA-3'; GAPDH F: 5'-TGACCTCAACTACATGGTCTACA-3'; R: 5'-GACTCCACGACATACTCAGCA-3'. RT-qPCR cycling parameters were optimised for each gene and were as follows:BRCA1, 400nM Forward and reverse primers, 45 cycles of 95 °C 15 s; 60 °C 40 s; 72 °C 20 s. TNFα and TNFR1, 500nM forward and reverse primers, 45 cycles of 95 °C 10 s; 60 °C 20 s; 72 °C 10 s. Amplicons were confirmed by analysis of melting peaks and agarose gel electrophoresis.

**mRNA Library preparation**

Four hundred ng of intact high quality total RNA (RIN>7.9) from each sample was then used as input to generate libraries for RNA-sequencing using the NEBNext Ultra II Directional kit (NEB, Cat.no: E7760S) following the manufacturer's recommendations. This protocol involved an initial step of mRNA selection using a poly-A isolation module (NEB, Cat.no: E7490) to select for mRNA with a mature polyA tail, followed by fragmentation prior to first cDNA synthesis and barcoding second-strand cDNA synthesised with indices for Illumina sequencing for final library amplification (10-cycles). The resulting libraries (342-421bp) were assessed on the Bioanalyzer 2100 for purity. The NEBNext Library Quant Kit for Illumina (NEB, Cat.no: E7630L) was used to calculate the quantity of each library. The quantification data was used to pool the libraries in equal molarity prior to performing a QC run on the MiSeq (MiSeq Reagent Kit v3 (150-cycle); Cat no: MS-102-3001). Further deep sequencing was performed on the pooled library over 2 lanes using a HiSeq4000 (by GENEWIZ) to generate roughly 26 million reads per sample.

**RNA-Seq Data Analysis**

Samples were aligned to the reference genome (Rattus_norvegicus Rnor_6.0.94) with Bowtie2(Langmead and Salzberg, 2012). Aligned sequenced reads per sample were associated to annotated genes with HTSeq (https://htseq.readthedocs.io/en/release_0.11.1/count.html), followed by an inter-sample quantile normalization to correct for technical differences. Differential expression analysis (relative to the samples issued from non-injured and vehicle treated animals) has been performed with Deseq2 (Love et al., 2014). Differentially expressed genes assessed in various conditions (non-injured +C286; Injured +vehicle; Injured +C286) were stratified over three major states (induced, repressed or non-differentially expressed) such that a total of 26 hypothetical combinatorial co-expression events were inferred. Among them,

only 8 appeared as biologically significant situations where the effect of the ligand C286 could be inferred (Figure 1G). To support this hypothesis, all combinatorial co-expression events were analyzed for Gene Ontology (GO) enrichment (DAVID bioinformatics resources),(Huang da et al., 2009) demonstrating relevant enrichment GO terms preferentially in the case of the selected biologically selected co-expression paths.

**Microglia cultures**

Primary mixed glial cultures were prepared as described previously (Goncalves et al., 2019b). Briefly, mixed glial cultures were obtained from the cortices of C57B/6 postnatal mice (P5–P8). Cultures were maintained at 37 °C (5% $CO_2$/95% $O_2$) in medium containing 15% fetal bovine serum (Invitrogen) and 1% penicillin-streptomycin (Sigma Aldrich) for 10–14 days. Microglial cells were then harvested by forceful shaking for 1 min by hand and plated on poly-d-lysine-coated glass coverslips or plastic six-well plates. To obtain reactive microglia, cells were treated with 100ng/ml lipopolysaccharides (LPS) for 3hr (Tarassishin et al., 2014) and then for another 3 hr with either: vehicle; C286 ($10^{-7}$ M); KU55933 (Hickson et al., 2004) (1μM, Abcam, ab120637) or C286 +KU55933.

**Immunochemistry and Antibodies**

Immunohistochemistry and cytochemistry were carried out as previously described (Goncalves et al., 2005). For the spinal cords: paraffin wax (Pwax) embedded tissues, were first dewaxed in xylene and 100% IMS, then heated in citric acid (10 mM, pH = 6), until boiling, then washed under a running tap for 5 min. For microglia cultures: cells were fixed for 15 min. with 4% PFA. Tissue sections or cells were washed 3x for 5 min each in PBS before incubation with primary antibody in PBS-0.02% Tween at 4ºC overnight. Primary antibody was removed by washing 3x for 5 min each in PBS. They were incubated in the secondary antibody for 1 hr. at

room temperature (RT) in PBS-0.02% Tween, and then washed in PBS 3x for 5 minutes. Antibodies used were: mouse monoclonal anti-βIII tubulin (G7121, Promega, 1:1000); goat polyclonal anti-Iba1 (ab107159, Abcam, 1:2,000); chicken polyclonal anti-Iba1 (ab139590, Abcam, 1:500); rabbit polyclonal anti-FZD10 (ab83044, Abcam, 1:500); rabbit polyclonal anti-BDNF (NBP1-46750, Novus Biologicals,1:1,000); chicken polyclonal anti-GFP (ab13970, Abcam, 1:400) mouse monoclonal anti-TNFα (ab1793, Abcam, 1:500); rabbit polyclonal anti-TNFR1 (ab58436, Abcam, 1:500); rabbit polyclonal anti-NGF 9ab6199, Abcam, 1:100); sheep polyclonal anti-CGRP (BML-CA1137, ENZO, 1;500); rabbit polyclonal anti-BRCA1 (ab191042; Abcam, 1:50); rabbit polyclonal anti-γH2AX (ab2893, Abcam, 1:5,000); mouse monoclonal anti-pATM (sc-47739, Santa Cruz Biotechnology,1:50) ; mouse monoclonal anti-NeuN (MAB377, Millipore, 1:1000); rabbit monoclonal anti-NeuN (#12943, Cell Signaling Technology, 1:3000); rabbit polyclonal anti-P2XR4 (APR-024, alomone labs, 1:20); rabbit polyclonal anti-Daxx (LS-B363**,** LSBio, 1:50). Secondary antibodies were AlexaFluor™ 594, AlexaFluor™ 488 (1:1000, Molecular Probes, Life Technologies) and AlexaFluor™ 647 (1:1000, Molecular Probes, Life Technologies). DAPI was used to stain nuclei (1 μg/mL, Sigma Aldrich).

**Immunochemistry quantification**

Quantification of protein levels by immunofluorescence (IF) was done as previously described (Herrmann et al., 2010). In brief, positively stained areas were quantified as the pixels of immunoreactivity above a threshold level per unit area using the Zeiss Zen blue edition software. The threshold value was set to include fluorescent positive signal and to exclude background staining. Threshold values for a given section and stain remained the same throughout the study and the quantifications were done by an operator blinded to the treatments.

**Confocal microscopy**

Multichannel fluorescence (DAPI–FITC–Texas Red filter set) images were captured using a Zeiss LSM 700 laser-scanning confocal microscope. For high magnification images, a 63 x oil-immersion Aprochromat objective (Carl Zeiss) was used. Settings for gain, aperture, contrast and brightness were optimized initially, and held constant throughout each study so that all sections were digitized under the same conditions of illumination. Channels were imaged sequentially to eliminate bleed-through, and multichannel image overlays were obtained using Adobe Photoshop 7.0 (Adobe Systems).

**Western blotting**

Spinal cord proteins were isolated from the phenol fraction remaining after QIAzol RNA extraction, according to the Qiagen user-developed protocol RY16. Briefly, the phenolic phase was treated with ethanol and the proteins precipitated by isopropanol. Protein pellets were sequentially washed with 0.3M guanidine-hydrochloride in 95% ethanol and 100% ethanol, air dried, then resuspended in 10M urea, 50mM DTT in water. Protein concentrations were measured by Coomassie-Bradford assays and proteins were separated by SDS-PAGE from 20µg aliquots loaded on to 12% (w/v) Bis-Tris polyacrylamide gels. For BDNF analysis the separated proteins were blotted to a 0.45µm pore size nitrocellulose membrane (BA85; Schleicher and Schuell) with a Trans-Blot SD Semi-Dry Transfer Cell (Bio-Rad Laboratories). The membrane was incubated in Odyssey® Blocking Buffer (PBS) (LICOR Bioscience) for 1 h at RT followed by an overnight incubation at 4°C with the primary antibody in blocking buffer. Anti-β-actin antibody was then added, for 1 h at room temperature (RT), after which the membrane was washed with PBS containing 0.1%v/v Tween-20 and incubated for a further 1 h at RT with secondary antibodies in blocking buffer. Finally, the membrane was washed as before and simultaneously scanned at 700nm and 800nm using an Odyssey® protein detection

system (LICOR Bioscience). Proteins were quantified using Image Studio Lite software (LICOR Bioscience) and normalized against β-actin. For the detection of BRCA1, proteins were transferred to a Hybond™-ECL membrane (GE Healthcare). The membrane was cut at the 76kD marker and both sections incubated in a blocking buffer consisting of 1% (w/v) BSA in TBS-Tween-20 (0.1%, v/v) for 1 h at RT followed by an overnight incubation at 4°C with anti-BDNF antibody added to the top section only. The top membrane was washed with TBS-Tween-20 (0.1% v/v) then incubated with a biotinylated secondary antibody for 1 h at RT, washed as before and incubated with ECL™ Western Blotting Detection Reagents (GE Healthcare). Proteins were visualised with the BioSpectrum Imaging system (UVP). The lower section of the membrane was incubated with a β-actin antibody for 1 h at RT followed by washing with TBS-Tween-20 (0.1% v/v) and incubation for a further at 1 h at RT with secondary antibodies in blocking buffer. β-Actin was visualised with the Odyssey® protein detection system (LICOR Bioscience) as above. Antibodies: Rabbit polyclonal anti-BRCA1 (ab191042, Abcam, 1:500); mouse monoclonal anti-BDNF (Ab205067, Abcam, 1:500); Rabbit polyclonal anti-β-actin (Ab8227, Abcam, 1:5000); Biotinylated Goat Anti-Rabbit IgG (BA-1000, Vector Laboratories, 1:500); Alexa Fluor680 (1:5000, Invitrogen) and IR Dye 800CW (1:5000, LICOR Biosciences).

**Statistical analysis**

Data and statistical analysis comply with the recommendations on experimental design and analysis in pharmacology (Curtis and Abernethy, 2015). Data analysis was performed in a blinded fashion. All statistical analysis was performed using Sigma Stat Software (SPSS Software Ltd, Birmingham, UK) using unpaired *t*-tests and one-way ANOVA with Pairwise Multiple Comparison Procedures (Tukey Test), or two-way ANOVA with Pairwise Multiple Comparison Procedures (Holm-Sidak method) as indicated in the Figure legends. $*p \leq 0.05$,

$^{**}p \leq 0.01$, $^{***}p \leq 0.001$. Exact p values are shown when p> 0.001. *n* represents the number of biological replicates. Experiments were repeated to ensure reproducibility of the observations. No statistical methods were used to predetermine sample size.

## Data and Software Availability

Raw and processed transcriptome datasets are available under the GEO accession number (GSE135080) and the Mendeley repository Mendeley Data, v1 **http://dx.doi.org/10.17632/kjvs5vgkbf.1**DOI .

## Supplemental references


Bennett, G.J., Chung, J.M., Honore, M., and Seltzer, Z. (2003). Models of neuropathic pain in the rat. Curr Protoc Neurosci *Chapter 9*, Unit 9 14.

Curtis, M.J., and Abernethy, D.R. (2015). Revision of instructions to authors for pharmacology research and perspectives: enhancing the quality and transparency of published work. Pharmacol Res Perspect *3*, e00106.

Goncalves, M.B., Boyle, J., Webber, D.J., Hall, S., Minger, S.L., and Corcoran, J.P. (2005). Timing of the retinoid-signalling pathway determines the expression of neuronal markers in neural progenitor cells. DevBiol *278*, 60-70.

Goncalves, M.B., Clarke, E., Jarvis, C.I., Barret Kalindjian, S., Pitcher, T., Grist, J., Hobbs, C., Carlstedt, T., Jack, J., Brown, J.T*., et al.* (2019a). Discovery and lead optimisation of a potent, selective and orally bioavailable RARbeta agonist for the potential treatment of nerve injury. Bioorg Med Chem Lett *29*, 995-1000.

Goncalves, M.B., Wu, Y., Clarke, E., Grist, J., Hobbs, C., Trigo, D., Jack, J., and Corcoran, J.P.T. (2019b). Regulation of myelination by exosome associated retinoic acid release from NG2-positive cells. J Neurosci.

Herrmann, J.E., Shah, R.R., Chan, A.F., and Zheng, B. (2010). EphA4 deficient mice maintain astroglial-fibrotic scar formation after spinal cord injury. Exp Neurol *223*, 582-598.

Hickson, I., Zhao, Y., Richardson, C.J., Green, S.J., Martin, N.M., Orr, A.I., Reaper, P.M., Jackson, S.P., Curtin, N.J., and Smith, G.C. (2004). Identification and characterization of a novel and specific inhibitor of the ataxia-telangiectasia mutated kinase ATM. Cancer Res *64*, 9152-9159.

Huang da, W., Sherman, B.T., and Lempicki, R.A. (2009). Bioinformatics enrichment tools: paths toward the comprehensive functional analysis of large gene lists. Nucleic Acids Res *37*, 1-13.

Kilkenny, C., Browne, W., Cuthill, I.C., Emerson, M., Altman, D.G., and Group, N.C.R.R.G.W. (2010). Animal research: reporting in vivo experiments: the ARRIVE guidelines. J Gene Med *12*, 561-563.

Langmead, B., and Salzberg, S.L. (2012). Fast gapped-read alignment with Bowtie 2. Nat Methods *9*, 357-359.

Love, M.I., Huber, W., and Anders, S. (2014). Moderated estimation of fold change and dispersion for RNA-seq data with DESeq2. Genome Biol *15*, 550.

McGrath, J.C., and Lilley, E. (2015). Implementing guidelines on reporting research using animals (ARRIVE etc.): new requirements for publication in BJP. Br J Pharmacol *172*, 3189-3193.

Tarassishin, L., Suh, H.S., and Lee, S.C. (2014). LPS and IL-1 differentially activate mouse and human astrocytes: role of CD14. Glia *62*, 999-1013.